Pergamon

PII: S0191-8141(97)00087-4

Journal of Structural Geology, Vol. 20, No. 4, pp. 385 to 405, 1998

0191-8141/98 $19.00 + 0.00

Finite strain and strain variation analysis in the Sheeprock Thrust Sheet: an internal thrust sheet in the Provo salient of the Sevier Fold-and-Thrust belt, Central Utah

MALAY MUKUL* and GAUTAM MITRA

Department of Earth and Environmental Sciences, University of Rochester, Rochester, NY 14627, U. S. A.

(*Received* 11 *December* 1996; *accepted in revised form* 19 *September* 1997)

Abstract—The Sheeprock thrust sheet in west-central Utah is an internal thrust sheet in the Provo salient of the Sevier fold-and-thrust belt. We have measured finite strain in quartzites (the dominant lithology), sampled along a square grid within the thrust sheet, using the modified normalized Fry method (McNaught, M. A. (1994) Modifying the normalized Fry method for aggregates of non-elliptical grains. *Journal of Structural Geology* **16** 493–503). The X/Y and X/Z axial ratios from unsampled locations within the sample area were estimated using the spatial statistics approach. The strain ellipsoids exhibit a variable three-dimensional orientation pattern resulting from modification of the initial layer parallel shortening (LPS) strain ellipsoid by fault parallel shear in conjunction with vertical flattening and/or horizontal stretching indicating that the thrust sheet did not undergo plane strain deformation in the transport plane. This suggests that the plane strain assumption used in drawing restorable balanced cross-sections breaks down for internal thrust sheets with more than one penetrative-strain producing deformation event. The X/Z strain axial ratios decrease away from the thrust towards the middle of the sheet. The X/Y strain axial ratios from interpolated image diagrams indicate transport-parallel stretching at the front end of the sheet and strike-parallel stretching at the back end of the sheet. The footwall and hanging wall finite strain patterns are similar indicating that most of the strain in the Sheeprock thrust sheet developed early in the deformation history of the thrust sheet before and perhaps during the growth of a large fault propagation fold pair. © 1998 Elsevier Science Ltd. All rights reserved

INTRODUCTION

The large-scale geometry of fold-and-thrust belts is fairly well established (Bally *et al.*, 1966; Dahlstrom, 1970; Boyer and Elliott, 1982; Woodward, 1985). Internal parts of fold-and-thrust belts are characterized by thrust sheets which commonly show strong penetrative deformation and folded thrusts which may be carrying basement (Mitra, 1978, 1979; Boyer and Mitra, 1988; Yonkee, 1992; Yonkee and Mitra, 1993). External thrust sheets commonly show little penetrative deformation (Mitra, 1994). Balancing techniques (Dahlstrom, 1969; Elliott, 1983) constrain the possible geometries in the external part of a fold-and-thrust belt by assuming that either the length or the area of individual beds or a combination of the two in the plane of section is conserved between the deformed section and the undeformed section (Woodward *et al.*, 1989; Mitra and Namson, 1989). Therefore, assumed deformation within an individual thrust sheet is limited to flexural-slip for line length balancing and plane strain for area balancing in two dimensions. Although these assumptions may be valid for the external part of fold-and-thrust belts, they clearly break down in internal thrust sheets where beds are penetratively deformed. Thus balanced cross-sections constructed across entire fold-and-thrust belts (FTBs) and their restorations will not be completely accurate.

One way to get around this problem is to include penetrative strain in the total displacement vector field for the emplacement of any thrust sheet (Mitra, 1994). Cross-sections must then be balanced by removing the translation (the slip) on the fault, rigid body rotation (represented by large scale dip changes due to large scale fault propagation and fault bend folds) and penetrative strain from the thrust sheet (Protzman and Mitra, 1990; McNaught and Mitra, 1996). However, questions about the validity of the basic assumptions in the construction of balanced cross-sections remain. For example, is the plane strain assumption made for the external part of FTBs still valid for the internal part of fold-and-thrust belts? Step-wise retro-deformation rather than restoration of balanced cross-sections has been suggested (Woodward *et al.*, 1989; Protzman and Mitra, 1990; Mitra, 1994; McNaught and Mitra, 1996) in thrust sheets exhibiting penetrative strain. However, this requires a detailed knowledge of the deformation that has occurred within each stratigraphic unit including well-developed incremental strain markers to determine the deformation path. Such detailed information is rarely available and commonly only finite strain markers are available. McNaught and Mitra (1996) suggest substituting a model path for the deformation path and applying it in reverse order to a cross-section to test if a viable (Elliott, 1983) restored section can be produced; they

*Present address: CSIR Centre for Mathematical Modelling and Computer Simulation, Bangalore 560 037, India.
E-Mail: mlym@cmmacs.ernet.in

used this approach to retrodeform and restore deformation in the Meade thrust sheet which is a transitional sheet in the foreland–hinterland transition of the Idaho–Utah–Wyoming salient of the Sevier fold-and-thrust belt.

Our objective in this paper is to examine the finite strain and strain variation patterns in an internal thrust sheet and study the implications of the results for cross-section balancing. Is the plane strain assumption valid for internal thrust sheets? If not, what parts of the thrust sheet violate this assumption? Is there a dominant, penetrative-strain producing deformation event in the thrust sheet or are there multiple events which have resulted in the observed finite strain pattern in the Sheeprock thrust sheet? Finally, is it at all possible to construct a meaningful retrodeformable cross-section from an internal thrust sheet? To answer these questions we will use the Sheeprock thrust sheet as an example. The Sheeprock thrust sheet is an internal thrust sheet in the Provo salient of the Sevier FTB in north-central Utah.

REGIONAL GEOLOGY

The Provo salient is a part of the Sevier orogenic belt in the North American Cordillera. A series of west-dipping thrust faults transported parts of the pre-existing Proterozoic, Paleozoic and Mesozoic miogeocline eastward during the late Cretaceous and early Tertiary Sevier orogeny (Fig. 1). Five major thrusts make up the Provo salient of the Sevier fold-and-thrust

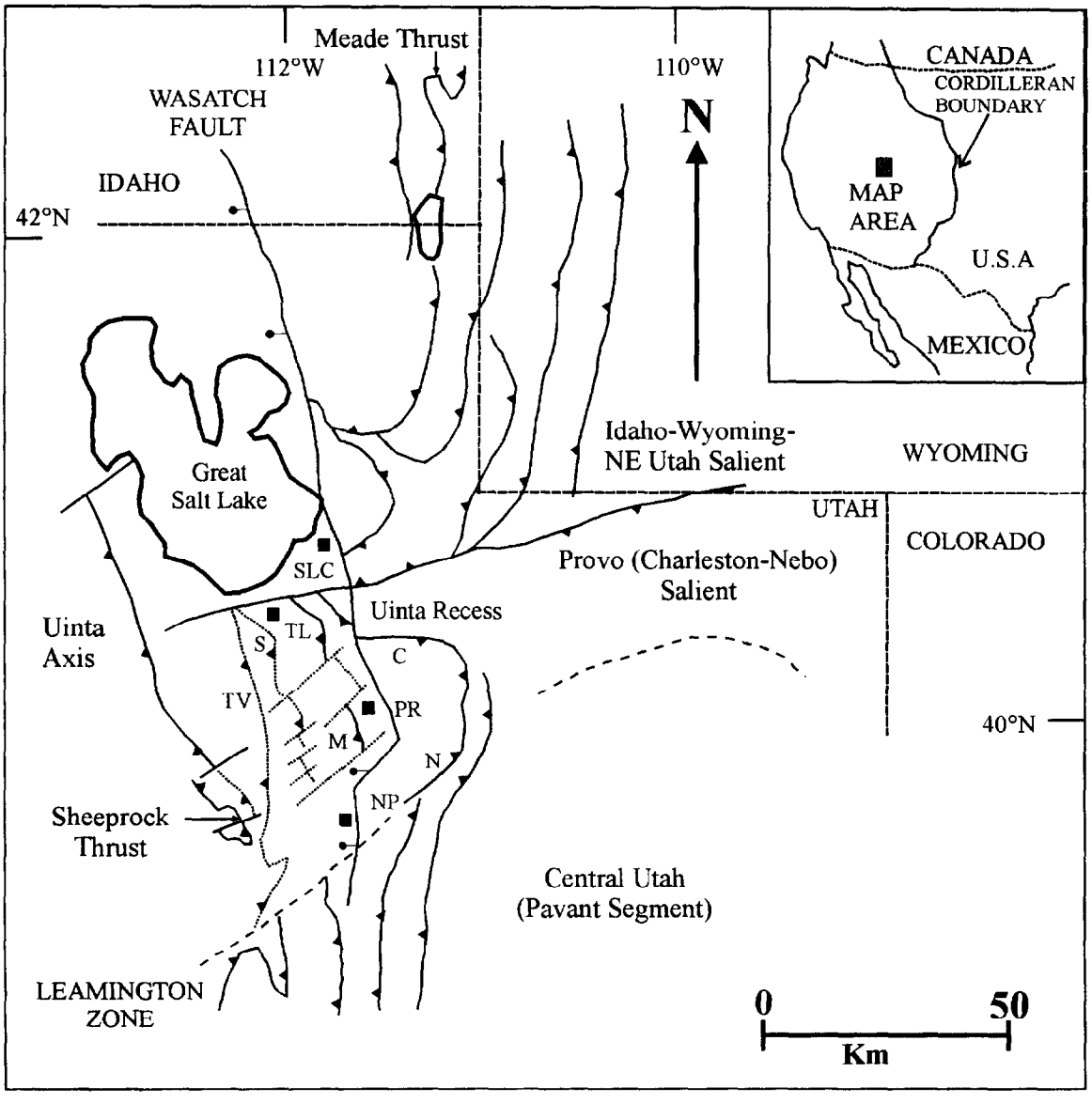

Fig. 1. Simplified map of the Sevier fold-and-thrust belt in Idaho–Wyoming and Northern Utah. Three salients separated by transverse zones are shown along with the positions of the major thrusts in the area. Symbols: SLC—Salt Lake City; TL—Tooele; PR—Provo; NP—Nephi; TV—Tintic Valley Thrust; S—Stockton Thrust; M—Midas Thrust; C—Charleston Thrust; N—Nebo Thrust.

belt. From west to east they are the Sheeprock thrust, the Tintic Valley thrust, the East Tintic–Stockton thrust system, the Midas thrust, the Charleston–Nebo thrust system, and frontal blind thrusts forming a triangle zone adjacent to the undeformed foreland (Wasatch Plateau) (Fig. 1) (Morris and Shepard, 1964; Black, 1965; Mabey and Morris, 1967; Morris and Lovering, 1979; Christie-Blick, 1983; Morris, 1983; Tooker, 1983; Smith and Bruhn, 1984; Lawton, 1985; Bruhn *et al.*, 1986; Mukul and Mitra, 1998a,b, submitted; Mitra, 1997). The timing of movement on these thrusts is not well known due to lack of direct evidence from synorogenic sediments. However, cross-cutting relationships and indirect relationships from synorogenic sediments indicates that thrusting in this salient probably occurred between Aptian (115 Ma) and Campanian–Paleocene (80–55 Ma) (Mitra, 1997). The major thrusts probably formed successively from west to east, with some reactivation in the back of the internal wedge (Jefferson, 1982; Lawton, 1985; Bryant and Nichols, 1988; Schwans, 1988; Mitra, 1997).

The structures of the Provo salient are, in general, typical of the "foothills family of structures" (Dahlstrom, 1970). Major thrust faults are listric and are asymptotic at depth with a low-angle basal decollement which is located at or above the basement-cover contact along much of its length (Mitra, 1997). The major thrusts carry Proterozoic sedimentary rocks in their hanging walls. However, the Charleston–Nebo thrust system carries Precambrian basement in its hanging wall (Bruhn *et al.*, 1986; Hintze, 1988) suggesting that the basal decollement cut down-section and incorporated a slice of basement into its hanging wall at or near the miogeocline-shelf hinge (Mitra, 1997). The basal decollement cuts up-section at the Charleston–Nebo thrust, climbing through the Paleozoic and lower part of the Mesozoic section to a Jurassic salt horizon (Lawton, 1985). Large-scale folding in the salient is dominated by fault propagation folds. Large-scale fault propagation folds involving the entire miogeoclinal sequence (Mitra, 1997) are seen in the Sheeprock (Mukul and Mitra, submitted), Midas (Tooker, 1983) and Nebo (Smith and Bruhn, 1984) thrust sheets. Although the overall shape of the major thrusts are listric, in detail they exhibit a ramp–flat geometry and large-scale fault bend folds are formed as the result of movement of hanging wall ramps onto footwall flats. Much of the deformation in this salient is confined to the miogeoclinal section and very little deformation extends on to the shelf (Levy and Christie-Blick, 1989; Mitra, 1997).

THE SHEEPROCK THRUST AND THRUST SHEET

The Sheeprock thrust is one of the major thrusts of the Provo salient. Its surface trace is exposed in the Sheeprock and the adjacent West Tintic Mountains in north-central Utah (Loughlin, 1920; Eardley, 1939; Stringham, 1942; Gardner, 1954; Cohenour, 1959; Groff, 1959; Morris and Kopf, 1970a,b; Christie-Blick, 1983; Mukul and Mitra, 1998a,b, submitted). Movement on the thrust is dated as Aptian (~97 115 Ma) (Mitra, 1997) though this date is not well constrained. It is the westernmost thrust observed in the Provo salient (Christie-Blick, 1983; Mukul and Mitra, 1998a,b) and the sheet carried by it exhibits penetrative style of deformation; the Sheeprock sheet is an internal thrust sheet in the salient. The Sheeprock thrust carries Proterozoic through Early Mesozoic sedimentary section in the hanging wall and is folded into a gentle anticline–syncline pair as a result of movement over a ramp on a later, lower thrust (Mukul and Mitra, submitted), most probably the Midas thrust or one of its hanging wall imbricates (Mitra, 1997). The evolution of the structure in the Sheeprock thrust sheet is explained by a series of schematic cross-sections (Fig. 2). A large, near recumbent, fault propagation fold involving Proterozoic through Mississippian sedimentary rocks is the major structure seen in the thrust sheet (Mukul and Mitra, 1998a,b, submitted) (Fig. 2b). The Sheeprock thrust cuts through the fault propagation antiform–synform pair preserving the antiform in the hanging wall and the synform in the footwall. Upright fold hinges in the Proterozoic Otts Canyon slates in the hanging wall of the Sheeprock thrust are related to fault bend folding in the sheet as a result of the movement of a hanging wall ramp onto a footwall flat in the Mississippian section (Fig. 2c). The ramp was subsequently tilted up on the forelimb of a fault bend fold on a lower, later thrust (Midas thrust, Mitra, 1997), producing a large-scale synform in the hanging wall of the Sheeprock thrust (Fig. 2d).

The Sheeprock thrust sheet was dissected by the Indian Springs fault (Fig. 3), a tear fault which was probably reactivated during Tertiary normal faulting. Part of the Sheeprock sheet south of the Indian Springs fault is downthrown and displaced to the west relative to the north (Mukul and Mitra, 1998a).

FINITE STRAIN ANALYSIS IN THE SHEEPROCK THRUST SHEET

Methods and overview

The Sheeprock thrust sheet is dominated by Proterozoic and Early Cambrian quartzites. The widespread occurrence of quartzites in the sheet allows finite strain to be determined from these quartzites using the center-to-center Fry Method (Fry, 1979; Erslev, 1988; Erslev and Ge, 1990; McNaught, 1994). The method used to calculate three dimensional strain ellipsoids from the quartzites in the Sheeprock thrust

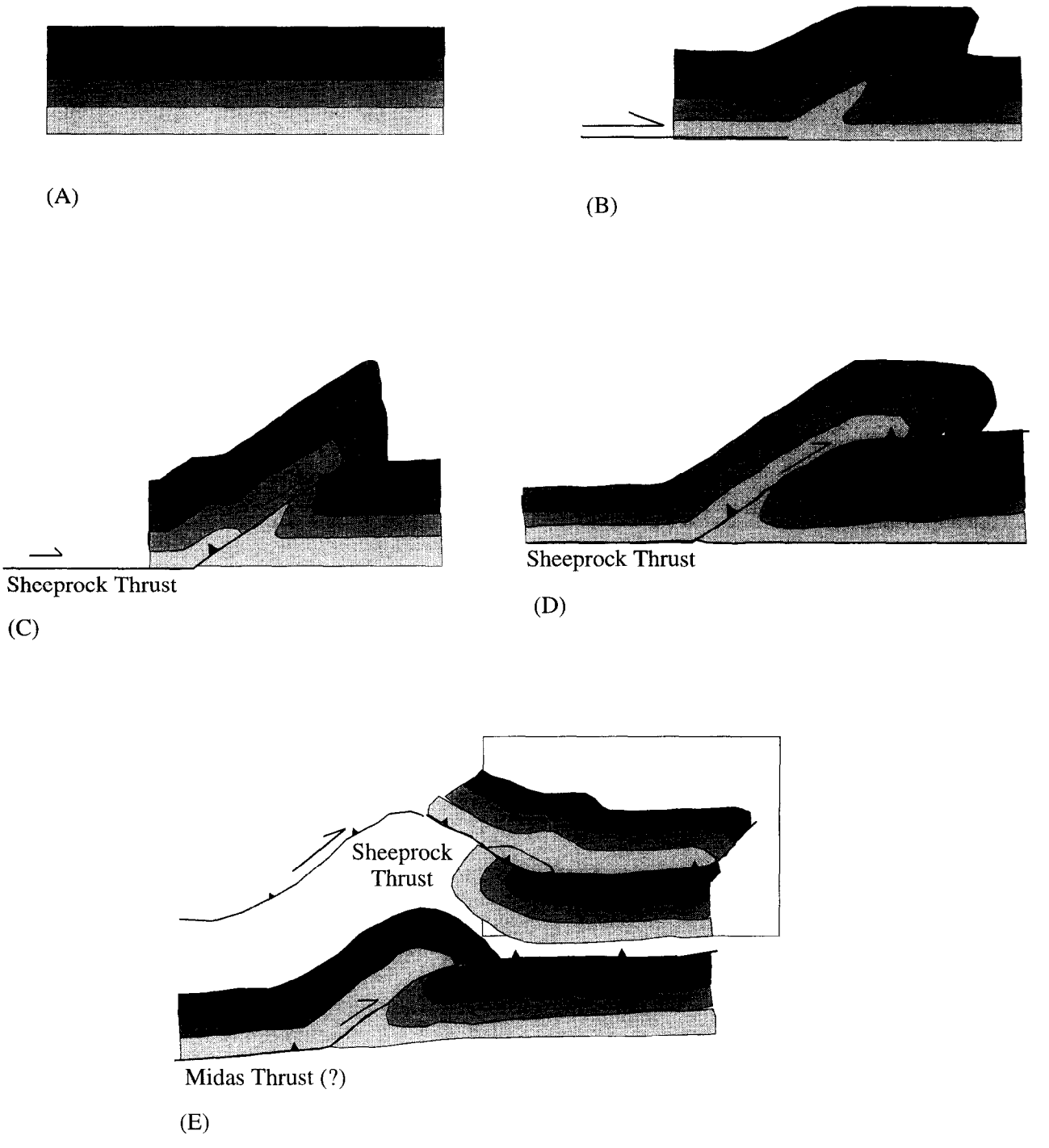

Fig. 2. A conceptual model to explain the evolution of the structures seen in the Sheeprock thrust sheet. The figures are schematic and not to scale. Fault propagation antiform–synform pair is developed once deformation initiates a fracture in the undeformed state (A) which propagates along a flat (B) and forms the Sheeprock thrust. The Sheeprock thrust climbs up-section by breaking through the common, overturned limb of the fault propagation antiform–synform pair preserving an overturned antiform in its hanging wall and an overturned synform in its footwall (C). Continued slip along the Sheeprock thrust and bending of the thrust to form an upper flat results in fault bend folding in the sheet (D). Fault bend folding over a younger thrust in the sub-surface (Midas (?), Mitra, 1997) folds the Sheeprock thrust such that the ramp is rotated and dips in the transport direction (E). The boxed part of figure (E) is the part of the structure from the Sheeprock thrust sheet preserved in the Sheeprock and the West Tintic Mountains.

sheet has been described in detail in the companion paper (Mukul, this issue). The axial ratios and the orientation of the three principal axes of the strain ellipsoid at each sample location are given in Appendix A. The X/Z strain axial ratio and the orientation of the long (X) axis of each finite strain ellipsoid were plotted on a map (Fig. 3).

The finite strain data in the Sheeprock thrust sheet was divided into three subsets to facilitate its analysis: hanging wall data north of the Indian Springs fault,

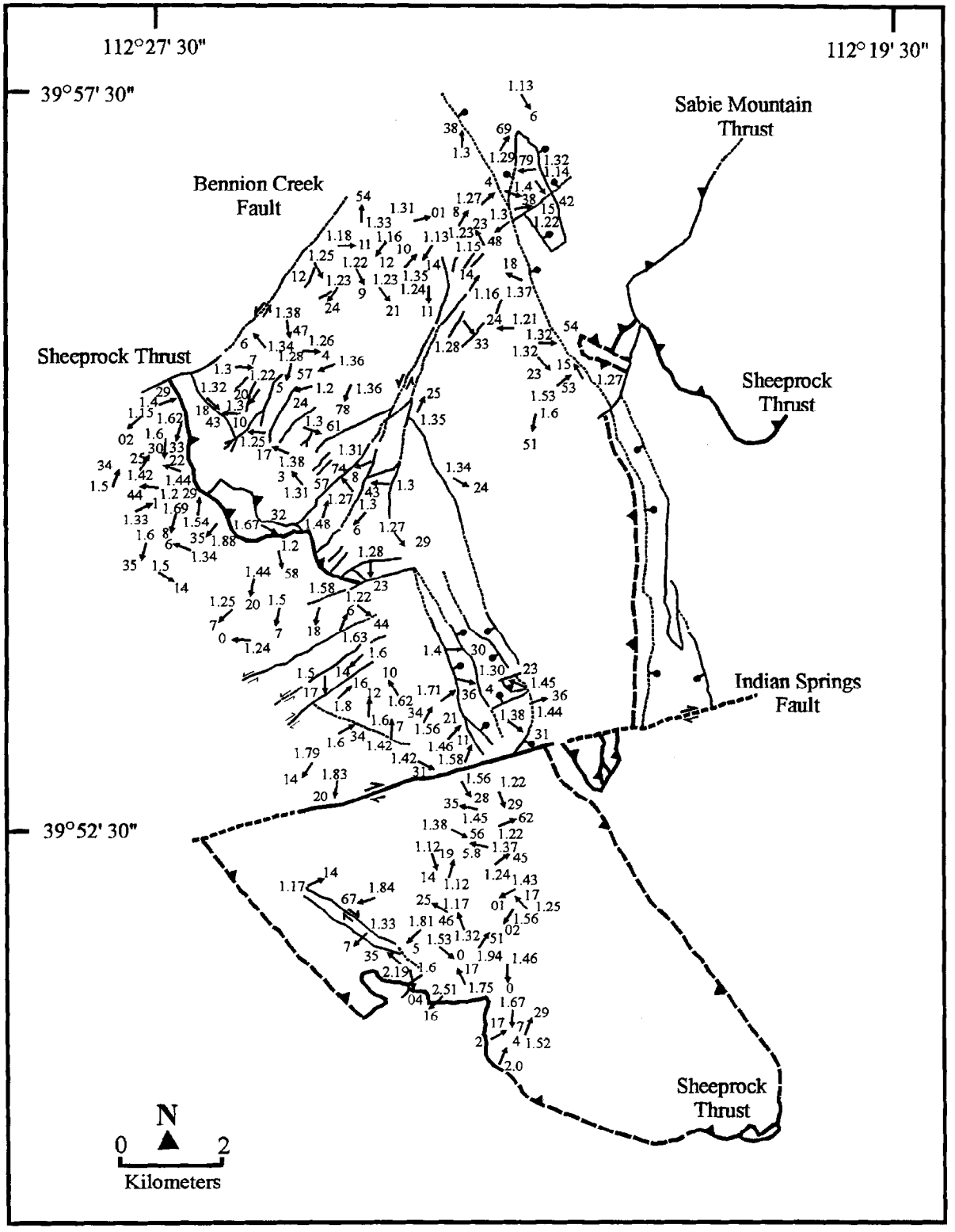

Fig. 3. Distribution of X/Z axial ratios and orientation of long axes (X) of finite strain ellipsoids in the Sheeprock thrust sheet. The X/Z ratio is written near the base of each arrow which represents the trend of the X axis at the sample location. Plunge of the X axis is written near the tip of each arrow. Solid fault lines represent exposed fault traces while dashed lines indicate fault traces interpreted from the exposed stratigraphy in the area.

footwall data north of the Indian Springs fault and hanging wall data south of the Indian Springs fault. The footwall of the synformally folded Sheeprock thrust south of the Indian Springs fault consists entirely of Paleozoic carbonates. This is also true for the footwall of the east limb of the folded Sheeprock thrust north of the Indian Springs fault. Therefore, footwall finite strain data are only available from the

footwall of the west limb of the folded Sheeprock thrust north of the Indian Springs fault (Fig. 2) where beds are overturned and mostly dip gently to the west.

Equal area stereograms of the orientations of the long (X), intermediate (Y) and short (Z) axes of the ellipsoids from the three areas in the sheet reveal that the overall X-axis orientations lie in a sub-horizontal plane but exhibit wide variation in their trends (Fig. 4). The overall intermediate (Y) axis orientations have steep to gentle plunges and exhibit variable trends (Fig. 4). The Z-axis, however, exhibits a high concentration near the vertical axis and generally lies very close to the regional transport plane. This indicates that of the three principal axes of the strain ellipsoids, Z exhibits the most consistent orientation.

Flinn diagrams of the finite strain ellipsoids from the thrust sheet (Fig. 5) show that in the hanging wall the ellipsoids vary from triaxial-oblate to triaxial-prolate. Samples close to the fault in the hanging wall and footwall of the Sheeprock thrust plot in the flattening field. In the footwall, most of the ellipsoids are triaxial-oblate.

Due to the variability of the finite strain data in the Sheeprock thrust sheet, it is best to look at the data with the transport plane as the frame of reference since this is the plane that is generally used for balanced section restorations. Since the short axis (Z) of the ellipsoid shows a consistent orientation and lies in the transport plane, its orientation is fixed in the transport plane; the other axis (which is perpendicular to Z) in the transport plane is chosen as X and the data in Appendix A is adjusted to reflect this. The "modified" data in the new reference frame are listed in Appendix B. The transport plane is now the X/Z plane in which the finite orientation of the Z axis is sub-vertical and the X axis sub-horizontal. This modification to the data allows a more comprehensive study of the finite strain variation in the Sheeprock

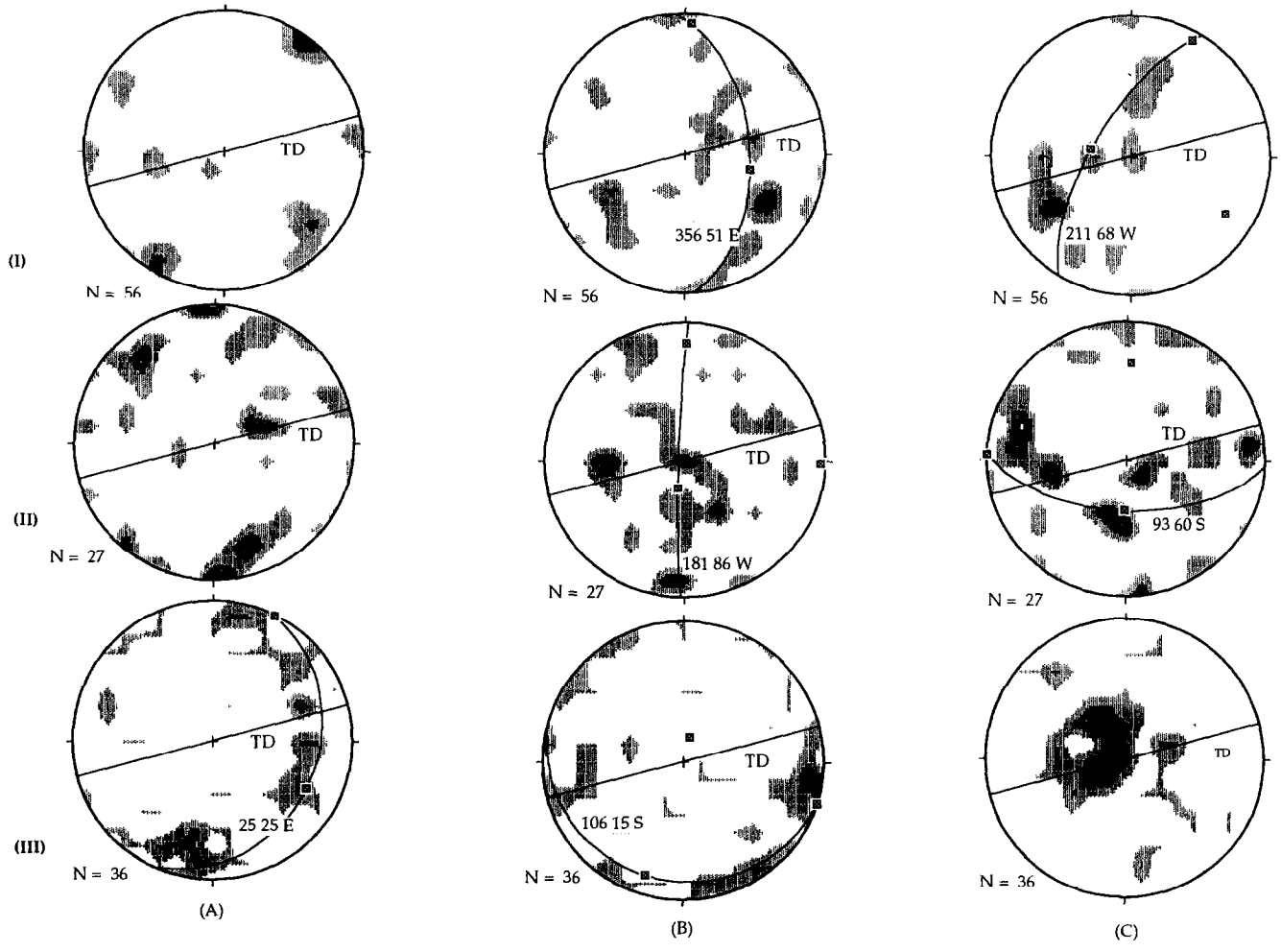

Fig. 4. Orientation of the three principal axes of the strain ellipsoid in the (I) hanging wall of the Sheeprock thrust sheet north of the Indian Springs fault (II) hanging wall of the Sheeprock thrust sheet south of the Indian Springs fault and (III) footwall of the Sheeprock thrust sheet north of the Indian Springs fault. The orientation of the long axis (X) is given in (A); the orientation of the intermediate axis (Y) is given in (B); and the orientation of the short axis (Z) is given in (C). The regional transport plane (TD) is shown on each stereogram.

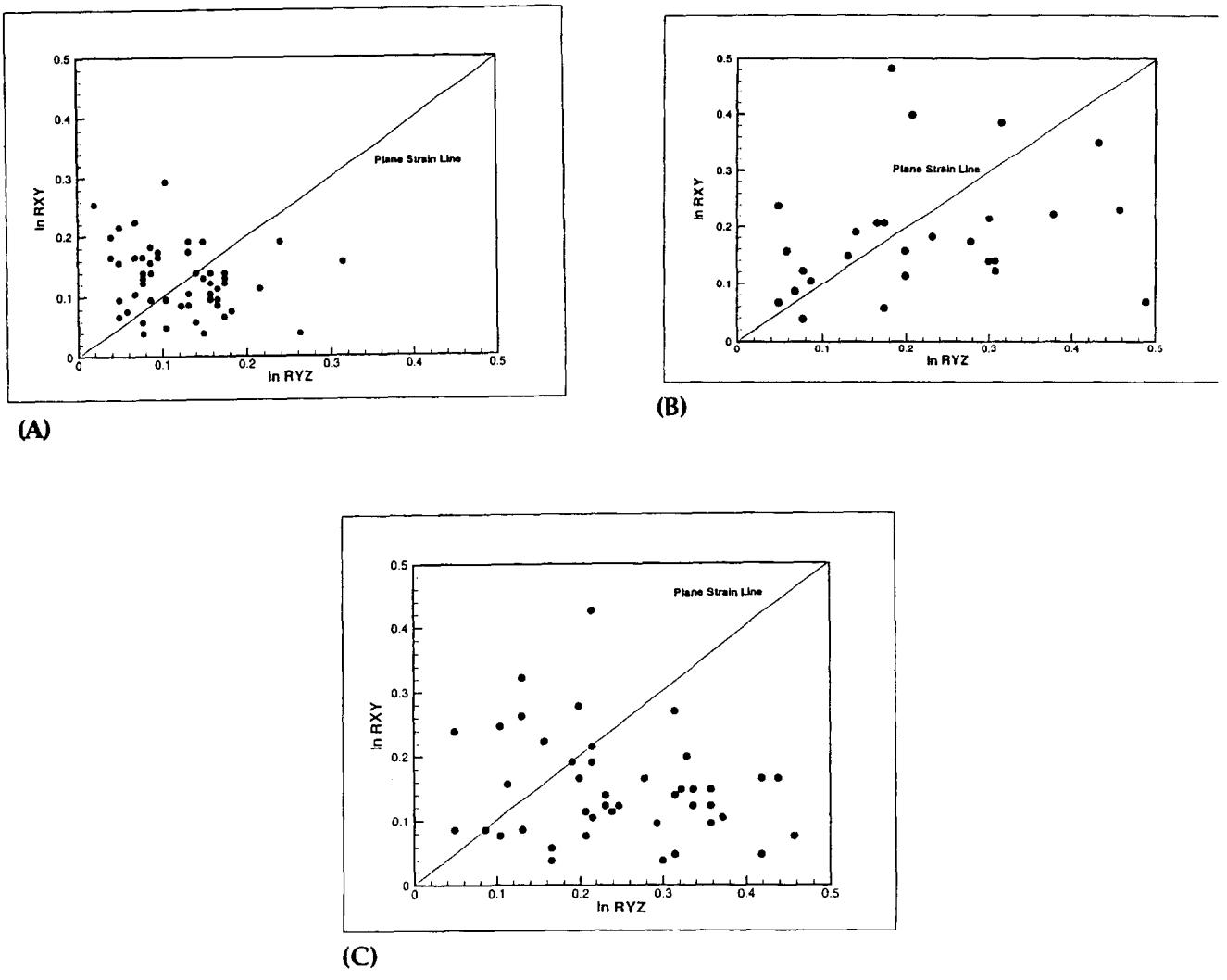

Fig. 5. Flinn diagrams of strain ellipsoids in the (A) hanging wall of the Sheeprock thrust north of the Indian Springs fault; (B) hanging wall of the Sheeprock thrust south of the Indian Springs fault; (C) footwall of the Sheeprock thrust north of the Indian Springs fault.

thrust sheet with reference to the strain variation in the transport plane.

"Modified" X/Y and X/Z axial ratios (Appendix B) were used to obtain kriged X/Y and X/Z interpolated image plots (using the software Transform by Spyglass) in plan view within the sampled areas. We prepared these plots using exponential semivariogram models as described in detail in the spatial statistics method discussed in the companion paper (Mukul, this issue). The finite strain observed in the Sheeprock thrust was also factorized into simple shear and stretch components by using the transport (downplunge) plane as the reference frame. Assuming there was no volume change, this was done by plotting the X/Z ratios (R) along the X-axis and the angle between the fault (shear direction) and the long axis (X) of the ellipsoid (i.e. θ') along the Y-axis of a plot representing the downplunge plane and containing simple shear and stretch contours (Sanderson, 1982, Fig. 5).

Finite strain data from the hanging wall of the Sheeprock thrust north of Indian Springs fault

Quartzite samples were collected from 56 sample locations in the hanging wall of the Sheeprock thrust north of the Indian Springs fault. The X/Y axial ratios in the sheet are variable (Fig. 6) but two broad trends are observed; there is a west to east increase in X/Y ratios from <1 (i.e. $X < Y$) near the west limb to >1 (i.e. $X > Y$) in the east limb of the folded Sheeprock thrust, and also from south to north near the west limb.

The X/Z ratios vary from 1.13 near the middle of the sheet to about 1.6 near the east limb of the folded Sheeprock thrust (as viewed on the surface from the thrust trace). The highest values observed near the west limb of the folded Sheeprock are around 1.5. This, however, is a minimum estimate of the maximum X/Z ratio in the west limb because Otts Canyon

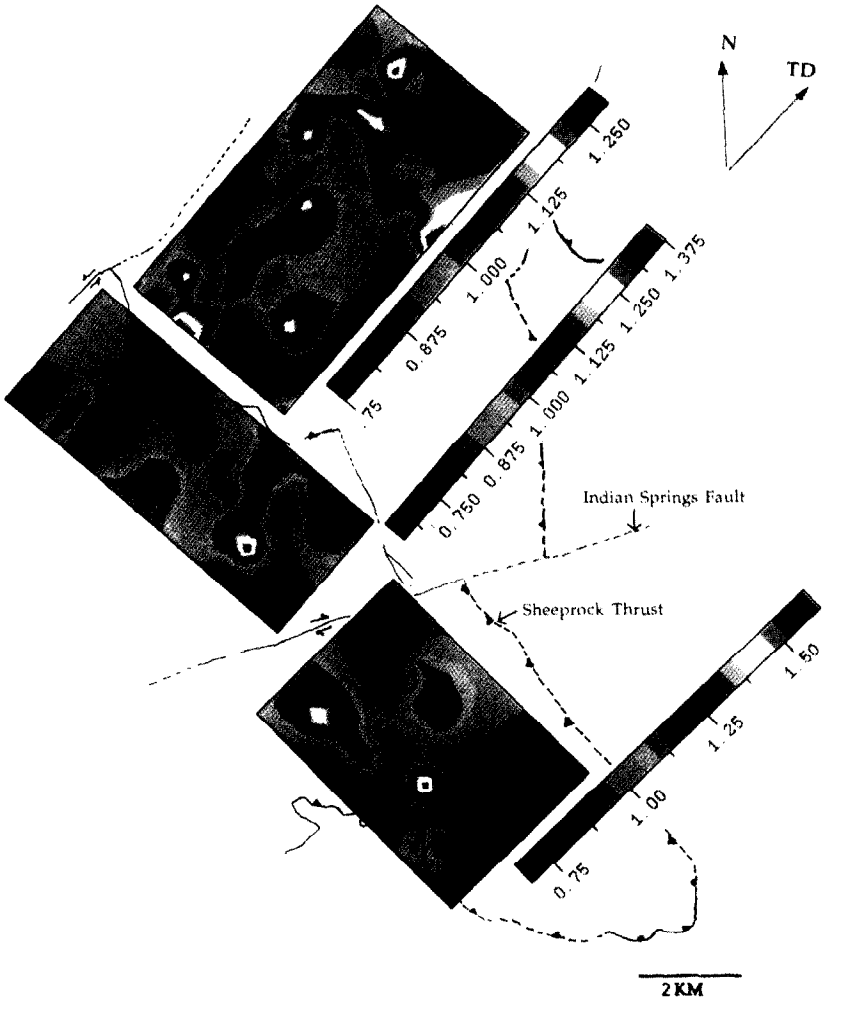

Fig. 6. Interpolated image plot of kriged modified X/Y (in plan) axial ratios in the folded Sheeprock thrust sheet. TD is the transport direction.

slates are present adjacent to the folded Sheeprock thrust and finite strain values are not available from this unit. The X/Z ratios vary both parallel and perpendicular to the approximately ENE–WSW transport direction (Fig. 7). In the transport direction, X/Z ratios increase from the middle of the sheet towards the thrust. Perpendicular to transport X/Z ratios increase from NW to SE towards the synformal closure of the folded Sheeprock thrust. However, the actual closure of the folded thrust is cut off by the Indian Springs fault. The highest X/Z ratios are observed near the east limb of the folded Sheeprock thrust from the west-dipping overturned limb of the fault-propagation antiform preserved in the hanging wall. These samples experienced flattening (Fig. 5).

The X/Z ratios were also kriged using an exponential semivariogram in the downplunge projection of the sheet along axis 4°, 325° to obtain the interpolated image diagram (Fig. 8) which corroborates the observations made in plan view (Fig. 7). An overall increase in the X/Z axial ratio is indicated from the middle to the base of the Sheeprock thrust sheet north of the Indian Springs fault. The maximum X/Z ratio in downplunge view occurs in the overturned limb of the fault-propagation antiform near the base of the sheet close to the east limb of the folded Sheeprock thrust.

Most of the samples from the hanging wall of the Sheeprock thrust exhibit low shear strain and low to medium stretch on a Sanderson plot (Fig. 9). The maximum shear strain (γ) is about 0.25 and the maximum stretch is 1.15. This implies that deformation does not take place by inhomogeneous simple shear alone; there is a significant component of stretching in the transport direction or flattening parallel to the thrust. A number of samples also plot above the $\alpha = 1$ line or in the $\alpha < 1$ field which implies that the long (X) axes in these samples is oriented at higher angles to the fault than would be expected for simple shear alone. These samples are located very close to the smaller scale fold hinges in the hanging wall suggesting that they reflect local shortening related to these folds.

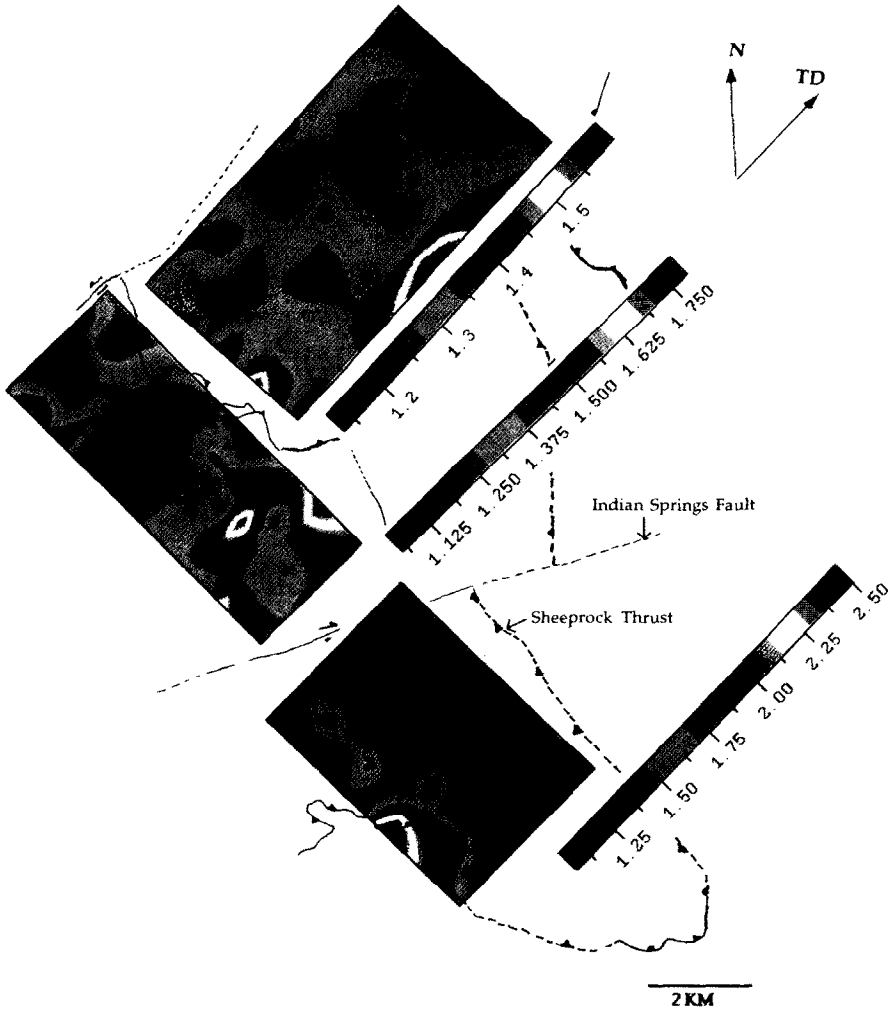

Fig. 7. Interpolated image plot of kriged modified X/Z (in plan) axial ratios in the Sheeprock thrust sheet. TD is the transport direction.

Finite strain data from the hanging wall of the Sheeprock thrust south of Indian Springs fault

The X/Y ratios in the sheet in this area ($N = 27$) were variable but are consistent with the trends observed in the X/Y ratios distribution in the hanging wall of the Sheeprock thrust north of the Indian Springs fault (Fig. 6). The data in the hanging wall south of the Indian Springs fault is concentrated near the back end of the sheet; the front end is covered by Cenozoic volcanics. The X/Y ratios increase north to south near the back end of the sheet indicating that the back of the Sheeprock thrust sheet was stretching perpendicular to transport both north and south of the Indian Springs fault. The X/Y ratios seem to increase towards the front end of the thrust but the lack of data near the east limb of the folded Sheeprock thrust does not allow confirmation of the trend. The low X/Y ratios near the western edge of the plot reflect low finite strain ratios from recrystallized samples.

The X/Z axial ratios (Fig. 7) vary from 1.05 near the middle of the sheet to about 2.51 near the west limb of the folded Sheeprock thrust in the hanging wall south of the Indian Springs fault. Finite strain could be calculated from quartzite close to the thrust in this case. The east limb of the folded thrust is not exposed and is covered by Cenozoic volcanics and Tertiary sediments.

Variation in X/Z ratios are observed both parallel and perpendicular to the approximately ENE–WSW transport direction as viewed on the surface (plan) (Fig. 7). In the transport direction, strain decreases from the thrust towards the middle of the sheet in plan view. Perpendicular to transport, X/Z ratios increase from N to S towards the closure of the synformally folded Sheeprock thrust. In the northwest part of the sampled area, the samples from the Otts Canyon Formation exhibit recrystallization and record lower strains. This is reflected in the low values recorded in the northwestern corner of the interpolated image plot. The highest X/Z ratios are observed near the west limb of the folded Sheeprock thrust. These samples also plot in the flattening field of the Flinn diagram (Fig. 5b).

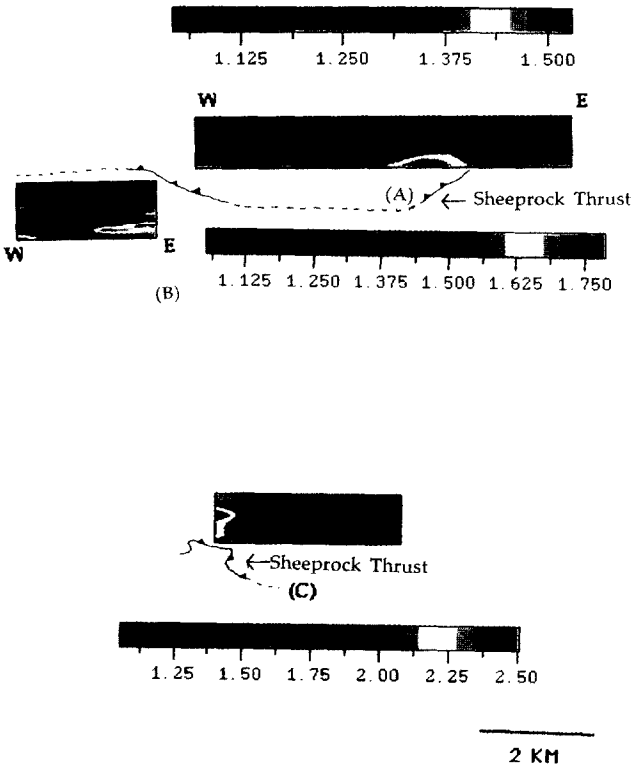

Fig. 8. Interpolated image plot of modified X/Z axial ratios in the Sheeprock thrust as seen in downplunge projection plane. The axis of downplunge projection is 4°, 325°.

The X/Z ratios were also kriged using an exponential semivariogram in the downplunge projection of the sheet along axis 4°, 325° to obtain the interpolated image diagram (Fig. 8). An overall increase in the X/Z axial ratio is indicated from the middle to the base of the Sheeprock thrust sheet south of the Indian Springs fault though the trend is not as well developed as observed in the hanging wall north of the Indian Springs fault. The maximum X/Z ratio in downplunge view is observed from samples near the west limb of the folded Sheeprock thrust.

On a Sanderson plot, most of the samples from the hanging wall of the Sheeprock thrust exhibit low shear strain and low to medium stretch (Fig. 10). In general, the shear strain (γ) is about 0.25 and the stretch is 1.1. A number of samples also plot in the $\alpha < 1$ field which implies that the long (X) axes in these samples are oriented at higher angles to the fault than would be expected for simple shear alone. These samples are also located very close to smaller scale fold hinges in the hanging wall indicating that their orientations may have been modified due to rotation due to smaller scale folding. A single sample taken very close to the thrust (about 5 m) exhibits shear strain (γ) of about 0.5 and maximum stretch of 1.5 (Fig. 10). This is close to the upper limit of the shear strain and stretch observed in the Sheeprock thrust sheet.

Finite strain data from the footwall of the west limb of the folded Sheeprock thrust north of Indian Springs fault

The X/Y axial ratios in the footwall in this region ($N = 36$) are variable (Fig. 6) but two broad trends are observed; there is an east to west increase in X/Y ratios from < 1 (i.e. $X < Y$) to > 1 (i.e. $X > Y$) away from the west limb of the folded Sheeprock thrust and also from north to south. This indicates that the footwall near the west limb of the folded Sheeprock thrust was stretching laterally similar to the immediately adjoining hanging wall. Farther away from the thrust the footwall was stretching in the transport direction. Variation in X/Z ratios is observed both parallel and perpendicular to the approximately ENE–WSW transport direction (Fig. 7). Highest X/Z values are observed near the thrust; X/Z ratios vary from 1.05 near the middle of the exposed footwall to about 1.8 near the west limb of the folded Sheeprock thrust. There is a decrease in strain away from the thrust near the middle of the exposed footwall along a southwesterly traverse (Figs 3 & 7). Strain values increase farther west. However, widespread recrystallization in the westernmost quartzite exposures prevents useful quantification of finite strain in the area. Perpendicular to the transport direction, strain increases from NW tc

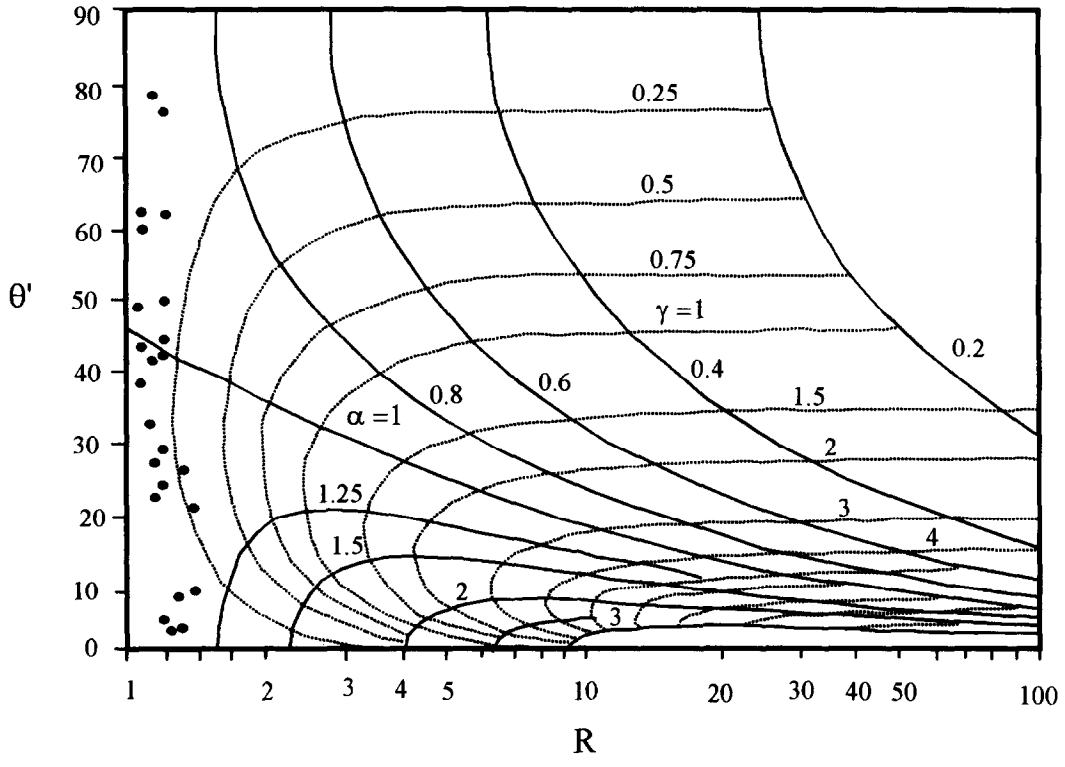

Fig. 9. The X/Z ratios (R) and angle of orientation of the X axis with the fault plane (θ') in downplunge view from the hanging wall north of the Indian Springs fault on a plot containing simple shear and stretch contours (Sanderson, 1982).

SE. Low X/Z values are recorded near the thrust near the central part of the plot. These samples are located near the hanging wall imbricate in the Sheeprock thrust (Fig. 3) and may have low strains because much of the shortening was taken up by the imbrication. Low X/Z ratios near the imbricate are also seen in the

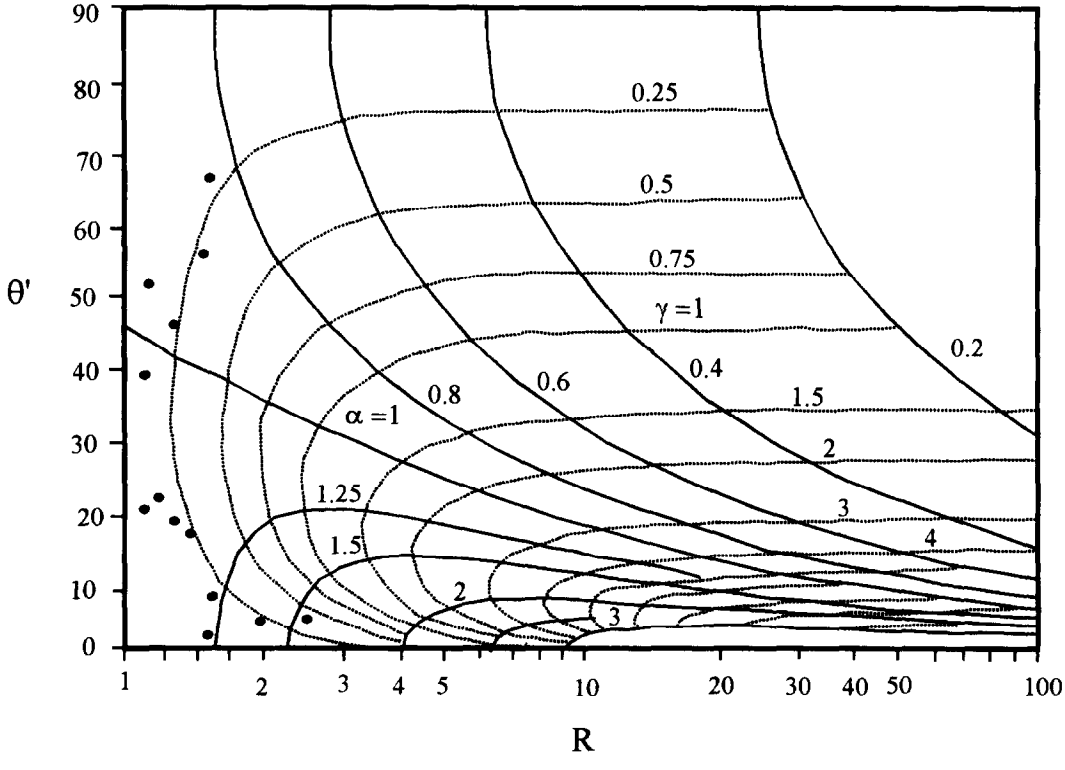

Fig. 10. The X/Z ratios (R) and angle of orientation of the X axis with the fault plane (θ') in downplunge view from the hanging wall south of the Indian Springs fault on a plot containing simple shear and stretch contours (Sanderson, 1982).

X/Z plot for the hanging wall of the Sheeprock thrust (Fig. 7).

The X/Z ratios were also kriged using an exponential semivariogram in a downplunge projection of the footwall along axis 4°, 325° to obtain the interpolated image diagram (Fig. 8). An overall increase in the X/Z axial ratio is indicated towards the base of the footwall of the Sheeprock thrust north of the Indian Springs fault. The finite strain distribution is complicated by the presence of recrystallized samples close to the fault which show low strains (Figs 3 & 8). Higher strains at the base of the footwall probably indicate that these rocks were close to a lower thrust in the subsurface; however, this interpretation would require an initial decrease in strain away from the Sheeprock thrust and then an increase in strain as the lower thrust is approached. The expected initial decrease in strain away from the Sheeprock thrust is not seen due to recrystallization and lower strains close to it.

On the Sanderson plot most of the samples from the footwall of the Sheeprock thrust exhibit low shear strain and low to medium stretch (Fig. 11). The maximum shear strain (γ) is about 0.5 and the maximum stretch 1.3. One sample plots in the stretch < 1 field. This sample is located very close to a smaller scale fold hinge where the Sheeprock thrust changes dip from moderately north-east to sub-horizontal so that it also reflects rotations related to smaller scale folding.

INTERPRETATION OF FINITE STRAIN DATA IN THE SHEEPROCK THRUST SHEET

The variation of X/Z axial ratios in the hanging wall and the footwall of the Sheeprock thrust sheet are similar to that observed in other fold-and-thrust belts throughout the world. The X/Z axial ratios are highest near the fault both in the footwall (1.8) and the hanging wall (2.51) (Fig. 3) and decrease away from the fault both in plan (Fig. 7) and in transport parallel cross-sections (Fig. 8). This pattern has been observed from many thrust sheets e.g. Bygdin area (Hossack, 1968), Blue Ridge (Mitra, 1979), the Morcles (Ramsay *et al.*, 1983), etc. The overall NW–SE increase in X/Z axial ratios observed in the Sheeprock thrust sheet (Figs 2 & 3) occurs due to the synformal folding of the thrust and the thrust sheet; X/Z axial ratios increase towards the synformal closure of the folded thrust.

Variation in the orientation of the long (X) axes of the strain ellipsoids is less commonly reported. McNaught and Mitra (1996) observed bedding-plane strain ellipses with long axes parallel to the transport direction from the Meade thrust sheet in the overturned section of the Jurassic Twin Creek Formation. Stretching parallel to transport has also been observed in the Willard thrust sheet (Yonkee, personal communication, 1996). Wojtal (Fig. 10; 1986) postulated a progressively thickening deformation zone near the base of external thrust sheets; this zone consisted of a

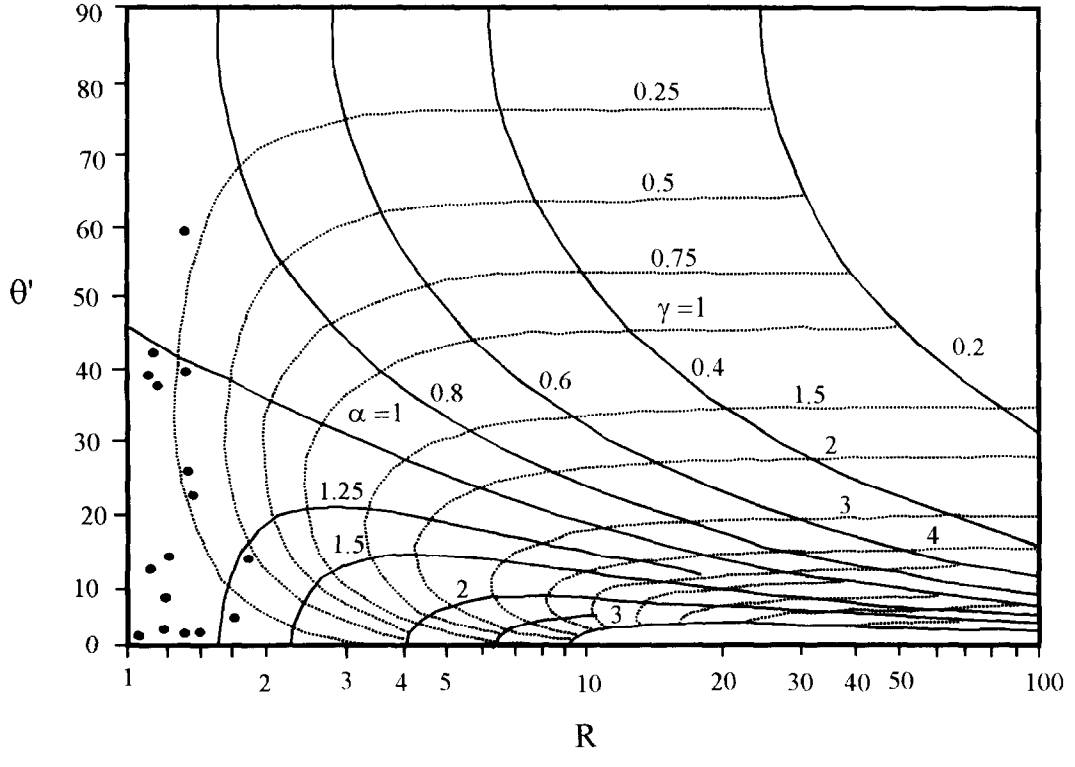

Fig. 11. The X/Z ratios (R) and angle of orientation of the X axis with the fault plane (θ') in downplunge view from the footwall north of the Indian Springs fault on a plot containing simple shear and stretch contours (Sanderson, 1982).

shortened and thickened zone which was underlain by a flattened and extended zone.

Cleavage orientations in the Sheeprock thrust sheet reveal that fault-parallel shear modified the LPS cleavage in the thrust sheet (Mukul and Mitra, submitted) and reduced the cleavage-bedding angle; thus the LPS strain ellipsoids were rotated. LPS strain ellipsoids in a thrust sheet are represented by strain ellipsoids whose long axes (X) lie in the transport plane and are approximately perpendicular to the transport direction which is sub-parallel to the short axis (Z) (Fig. 12). The intermediate axis (Y) is perpendicular to the transport plane. Since the LPS strains are low, a statistical distribution of ellipsoid shapes

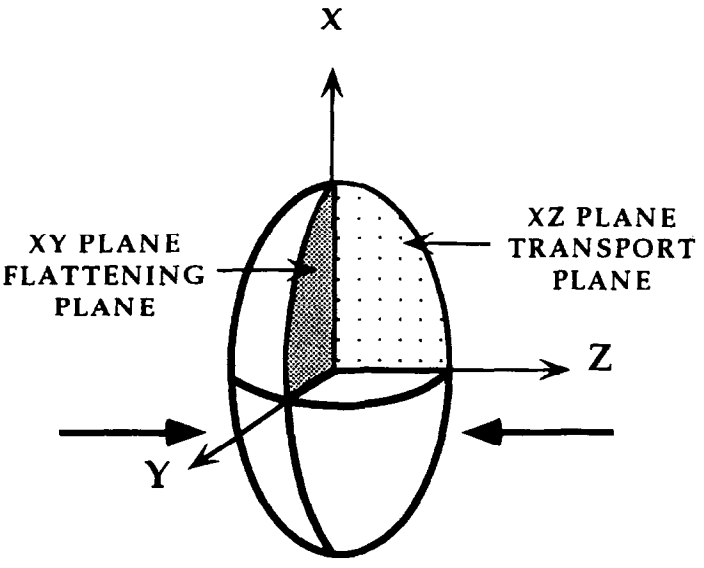

LPS STRAIN ELLIPSOID

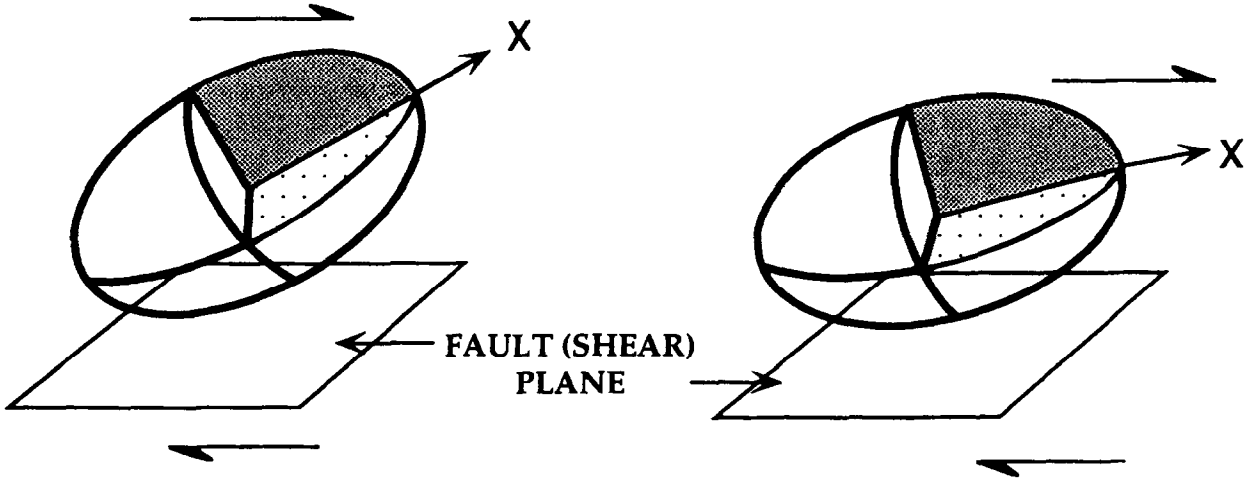

LPS ELLIPSOID MODIFIED BY FAULT PARALLEL SHEAR

FINITE STRAIN ELLIPSOID

Fig. 12. Schematic conceptual diagram to explain the development of finite strain pattern observed in the Sheeprock thrust sheet. LPS strain ellipsoid is formed as a result of initial layer parallel shortening in the sheet.

and orientations would be observed around the LPS strain ellipsoid shown in Fig. 12. Fault-parallel shear would rotate the LPS flattening plane (XY) closer to the fault and thereby decrease the angle the X-axis makes with the fault plane. Fault parallel shear acting on a statistical distribution of LPS ellipsoids would result in the variation in the plunge of the X axes. Near the thrust or in the overturned limb of the fault propagation fold where the shear strain is maximum, the XY or the flattening plane of the modified LPS strain ellipsoid will be sub-parallel to the thrust plane and X and Y axes will be sub-horizontal. Stretching near the thrust and in the overturned limb of the fault propagation fold causes further elongation of X and Y axes in the XY or the flattening plane. Thus, depending on the shape and the orientation of the ellipsoid, the finite ellipsoid can have X greater than, less that or equal to Y. The net effect of this would be a three-dimensional variation of X axis orientations such as that observed in the Sheeprock thrust sheet (Fig. 13); the flattening plane is sub-horizontal in the overturned limb in the footwall and Z' is vertical (Fig. 4) and samples near the thrust and on (and near) the overturned limb exhibit oblate finite strain ellipsoids (Fig. 5).

The variation in X/Y ratios in the Sheeprock thrust sheet indicate that the front limb of the Sheeprock thrust was stretching in the transport direction while the back limb was stretching laterally (Fig. 6). The manner in which stretching was distributed in the thrust sheet would have influenced the shape of the frontal boundary of the evolving thrust belt in plan. If there were a smooth gradation from the frontal transport-parallel stretching to the transport-perpendicular stretching at the back end of the sheet, the frontal boundary would be smooth and curvilinear. If, on the other hand, the transition were not gradational, a strongly-arcuate, almost tongue-shaped frontal boundary would result. In addition, due to the abrupt transition, tensile microscopic fractures would develop in the transition zone which would be accentuated by fault-parallel shear to form transport-parallel tear faults or lateral zones. The Charleston–Nebo salient exhibits a strongly-arcuate, almost tongue-shaped frontal boundary (Fig. 1). The tongue-shaped frontal boundary is bounded by lateral zones and tear faults are also present in the salient on all scales (Christie-Blick, 1983; Mitra, 1997). The Sheeprock thrust sheet also exhibits a large number of transport parallel tear faults. These observations indicate that the stretching distribution did not vary smoothly or there were gradients in the distribution of stretching in the Sheeprock sheet and consequently, the Charleston–Nebo salient developed a strong arcuate shape.

The footwall and the hanging wall of the Sheeprock thrust show similar strains; this indicates that most of the strain was produced early in the deformation history of the Sheeprock thrust before the thrust cut through the fault-propagation structure. Very little strain is produced by fault-bend folding in the sheet; only samples close to the smaller scale fault-bend fold hinges seem to show related strains.

In summary, the finite strain ellipsoids observed in the Sheeprock thrust are the result of the modification of an initial LPS strain ellipsoid by fault-parallel shear accompanied by flattening and/or stretching. The shape of the finite strain ellipsoid depends mainly on two factors; the shape and orientation of the LPS strain ellipsoid and the amount of fault parallel shear which controls the orientation of the flattening (X/Y) plane of the LPS strain ellipsoid with respect to the fault plane. Variation of these factors in the Sheeprock thrust sheet result in the finite strain pattern observed in the sheet.

IMPLICATIONS OF FINITE STRAIN ANALYSIS IN THE SHEEPROCK THRUST SHEET IN CROSS-SECTION RETRODEFORMATION

Cross-section balancing and retrodeformation techniques in external and transitional portions of fold-and-thrust belts have assumed that the deformation in fold-and-thrust belts is plane strain. Typically, there is a dominant penetrative strain producing deformation event in the thrust sheet; the intermediate axis (Y) of the strain ellipsoid is perpendicular to the transport plane which contains the long (X) and the short (Z) axes with Z being parallel to transport (Mitra, 1994). If plane strain is assumed in sections parallel to the transport direction, the appropriate shortening values in the plane of section can be calculated and used to remove penetrative shortening in the thrust sheet.

Most of the above criteria are not satisfied in the Sheeprock thrust sheet. First, there are three dominant penetrative strain producing events in the sheet: fault parallel-shear accompanied by stretch modifies an earlier LPS strain. Their interaction results in a three dimensional finite strain distribution in the thrust sheet which violates the plane strain assumption in the overall ENE–WSW transport direction. If, however, incremental strain data were available such that the penetrative strain produced by both events could be separately quantified, the plane strain assumption could be made individually for deformation perpendicular and parallel to transport and shortening individually removed from the thrust sheet. Therefore, a three-dimensional retrodeformation would be the only meaningful way to proceed. However, the problem of three-dimensional retrodeformation of penetratively deformed thrust sheets is yet to be addressed successfully.

Studies in the Sheeprock thrust sheet reveal that it may not be possible to construct meaningful retrodeformable cross-sections from internal thrust sheets using just finite strain data. Internal thrust sheets typi-

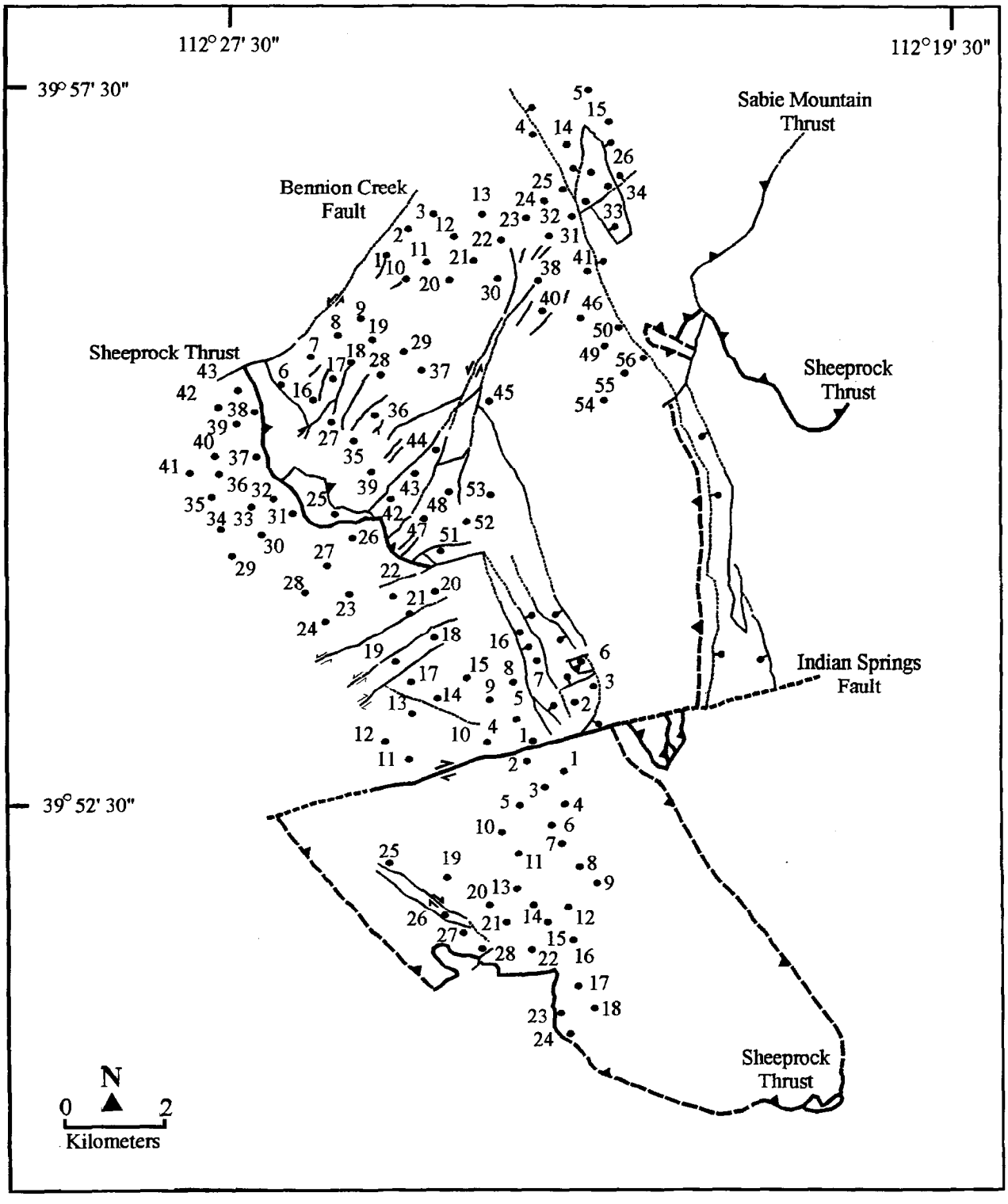

Fig. 13. Sample locations for data in Appendix A.

cally deform at higher P–T conditions than external or transitional thrust sheets. They are also subjected to multiple deformation episodes; one or more of these events may be penetrative strain producing deformation events. Although, these deformation events may individually satisfy plane strain condition, their interaction with each other would probably result in a non-plane strain three-dimensional strain distribution. Incremental strain data may help separate individual penetrative-strain causing deformation events quantitatively and allow the removal of their effects on the thrust sheet individually. However, in the absence of incremental strain data, meaningful retrodeformation of internal thrust sheets may not be possible until three dimensional retrodeformation techniques for removal of penetrative strain from thrust sheets are

developed. The best possible approach to the problem at the present time would be to define a "model path" for retrodeformation (McNaught and Mitra, 1996) which would allow non-planar finite strain distribution.

This "model path" approach can be extended and forward modeling, using numerical techniques such as finite element methods can be used to supplement the finite strain data obtained using spatial statistics. This would provide a possible model deformation path that will simulate the finite strain distribution presented here. The numerical model(s) must be constrained by real world observations and strain data presented in this paper. This might prove to be a viable option to try and understand the mechanics of fold-and-thrust belt evolution in the absence of three-dimensional retrodeformation techniques for removal of penetrative strain from thrust sheets. We are currently investigating this approach and the results of this study will be published elsewhere.

Acknowledgements—This paper is an outgrowth of a doctoral dissertation done at the University of Rochester. This work was supported by NSF grant EAR-9418688 to G. Mitra and by grants from the American Association of Petroleum Geologists (Peter W. Gester Memorial Grant), the Geological Society of America, and Sigma Xi to M. Mukul. Reviews by Mike Bradley and D. Wiltschko helped strengthen the paper. Stereograms used in the paper were generated using Richard Allmendinger's program Stereonet.

REFERENCES

Bally, A. W., Gordy, L. and Stewart, G. A. (1966) Structure, seismic data and orogenic evolution of southern Canadian Rocky Mountains. *Bulletin of Canadian Petroleum Geology* **14**, 337–381.

Black, B. A. (1965) Nebo overthrust, southern Wasatch Mountains, Utah. *Brigham Young University Geologic Studies* **12**, 55–89.

Boyer, S. E. and Elliott, D. (1982) Thrust systems. *American Association of Petroleum Geologists Bulletin* **66**, 1196–1230.

Boyer, S. E. and Mitra, G. (1988) Deformation of the basement-cover transition zone of the Appalachian Blue Ridge Province. In *Geometry and Mechanisms of Thrusting, with special reference to the Appalachians*, eds G. Mitra and S. Wojtal. pp. 119–136. Geological Society of America Special Paper, **222**.

Bruhn, R. L., Picard, M. D. and Isby, J. S. (1986) Tectonics and sedimentology of the Uinta Arch, western Uinta Mountains, and Uinta Basin. In *Paleotectonics and sedimentation in the Rocky Mountain region, United States*, ed. J. A. Peterson, pp. 333–352. American Association of Petroleum Geologists Memoir, **41**.

Bryant, B. and Nichols, D. J. (1988) Late Mesozoic and early Tertiary reactivation of an ancient crustal boundary along the Uinta trend and its interaction with the Sevier orogenic belt. In *Interaction of the Rocky Mountain Foreland and Cordilleran thrust belt*, eds W. J. Perry and C. J. Schmidt, pp. 119–141. Geological Society of America Memoir, **171**.

Christie-Blick, N. H. (1983) Structural geology of the southern Sheeprock Mountains, Utah: Regional significance. In *Tectonic and Stratigraphic studies in the Eastern Great Basin*, eds D. M. Miller, V. R. Todd and K. A. Howard, pp. 101–124. Geological Society of America Memoir, **157**.

Cohenour, R. E. (1959) Sheeprock Mountains, Tooele and Juab Counties: Precambrian and Paleozoic stratigraphy, igneous rocks, structure, geomorphology and economic geology. *Utah Geological and Mineralogical Survey Bulletin* **63**, 201.

Dahlstrom, C. D. A. (1969) Balanced cross sections. *Canadian Journal of Earth Science* **6**, 737–757.

Dahlstrom, C. D. A. (1970) Structural Geology in the eastern margin of the Canadian Rocky Mountains. *Bulletin of Canadian Petroleum Geology* **18**, 332–406.

Eardley, A. J. (1939) Structure of the Wasatch Great Basin region. *Geological Society of America Bulletin* **50**, 1277–1310.

Elliott, D. (1983) The construction of balanced cross-sections. *Journal of Structural Geology* **5**, 101.

Erslev, E. A. (1988) Normalized center-to-center strain analysis of packed aggregates. *Journal of Structural Geology* **10**, 201–209.

Erslev, E. A. and Ge, H. (1990) Least-squares center-to-center and mean object ellipse fabric analysis. *Journal of Structural Geology* **12**, 201–209.

Fry, N. (1979) Random point distribution and strain measurement in rock. *Tectonophysics* **60**, 89–105.

Gardner, W. C. (1954) Geology of the West Tintic mining district and vicinity, Juab County, Utah. Unpublished M. S. dissertation. *University of Utah* 43 pp.

Groff, S. L. (1959) Geology of the West Tintic Range and vicinity, Tooele and Juab Counties, Utah. Unpublished Ph. D. thesis. *University of Utah* 183 pp.

Hintze, L. F. (1988) Geologic history of Utah. *Brigham Young University Geology Studies Special Publication* **7**, 202.

Hossack, J. R. (1968) Pebble deformation and thrusting in the Bygdin area (Southern Norway). *Tectonophysics* **5**, 315–339.

Jefferson, W. S. (1982) Structural and stratigraphic relations of Upper Cretaceous to Lower Tertiary orogenic sediments in the Cedar Hills, Utah. In *Overthrust belt of Utah*, ed. D. L. Nielson, pp. 65–80. Utah Geological Association Publication, **10**.

Lawton, T. (1985) Style and timing of the frontal structures, Sevier thrust belt, central Utah. *American Association of Petroleum Geologists Bulletin* **69**, 1145–1159.

Levy, M. and Christie-Blick, N. (1989) Pre-Mesozoic palinspastic reconstruction of the eastern Great Basin (western United States). *Science* **245**, 1454–1462.

Loughlin, G. F. (1920) Sheeprock Mountains. In *The ore deposits of Utah*, ed. B. S. Butler, G. F. Loughlin and V. C. Heikes, pp. 423–444. U. S. Geological Survey Professional Paper, **111**.

Mabey, D. R. and Morris, H. T. (1967) Geologic interpretation of gravity and aeromagnetic maps of Tintic Valley and adjacent areas, Tooele and Juab counties, Utah. *United States Geological Survey Professional Paper* **516**(D), 1–10.

McNaught, M. A. (1994) Modifying the normalized Fry method for aggregates of non-elliptical grains. *Journal of Structural Geology* **16**, 493–503.

McNaught, M. A. and Mitra, G. (1996) The use of finite strain data in constructing a retrodeformable cross-section of the Meade thrust sheet, southeastern Idaho. *Journal of Structural Geology* **18**, 573–583.

Mitra, G. (1978) Ductile deformation zones and mylonites: The mechanical processes involved the deformation of crystalline basement rocks. *American Journal of Science* **278**, 1057–1084.

Mitra, G. (1979) Ductile deformation zones in Blue Ridge basement basement and estimation of finite strains. *Geological Society of America Bulletin* **90**, 935–951.

Mitra, G. (1994) Strain variation in thrust sheets of the Sevier fold-and-thrust belt, Idaho–Utah–Wyoming: Implications for section restoration and wedge taper evolution. *Journal of Structural Geology* **16**, 585–602.

Mitra, G. (1997) Evolution of Salients in a Fold-and-Thrust Belt: the Effects of Sedimentary Basin Geometry, Strain Distribution and Critical Taper. In *Evolution of geologic structures from macro- to micro-scales*. Ed. S. Sengupta, Chapman and Hall, London, 59–90.

Mitra, S. and Namson, J. S. (1989) Equal-area balancing. *American Journal of Science* **289**, 563–599.

Morris, H. T. (1983) Interrelations of thrust and transcurrent faults in the central Sevier orogenic belt near Leamington, Utah. *Geological Society of America Memoir* **157**, 75–81.

Morris, H. T. and Kopf, R. W. (1970a) Preliminary geologic map and cross-section of the Cherry Creek Quadrangle and adjacent part of the Dutch Peak Quadrangle, Juab County, Utah, U. S. Geological Survey Open-File Map, scale 1:24,000.

Morris, H. T. and Kopf, R. W. (1970b) Preliminary geologic map and cross-section of the Maple Peak Quadrangle and adjacent part of the Sabie Mountain Quadrangle, Juab county, Utah. U. S. Geological Survey Open-File Map, scale 1:24,000.

Morris, H. T. and Lovering, T. S. (1979) *General geology and mines of the East Tintic mining district, Utah and Juab counties, Utah.* U. S. Geological Survey, Professional Paper, 1024.

Morris, H. T. and Shepard, W. M. (1964) *Evidence for a concealed tear fault with large displacement in the central East Tintic Mountains, Utah.* U. S. Geological Survey Professional Paper 501C, pp. C19–C21.

Mukul, M. (1998) A Spatial Statistics approach to the quantification of finite strain variation in penetratively deformed thrust sheets: an example from the Sheeprock thrust sheet, Utah. *Journal of Structural Geology* **20,** 371–384.

Mukul, M. and Mitra, G. (1998a) Controversies in the geology of the Sheeprock thrust sheet, Sevier fold-and-thrust belt, Utah—A re-examination based on new evidence. In *Geology of the Sheeprock thrust sheet, Utah—New insights.* Utah Geological Survey Miscellaneous Publication **98-1**, Chapter 1, 56p.

Mukul, M. and Mitra, G. (1998b) Stratigraphy and structural geology of the southern Sheeprock and the adjacent West Tintic Mountains, Utah—A review and new interpretations based on structural analysis. In *Geology of the Sheeprock thrust sheet, Utah—New insights.* Utah Geological Survey Miscellaneous Publication **98-1**, Chapter 2, 56p.

Protzman, G. M. and Mitra, G. (1990) Strain fabrics associated with the Meade thrust: implications for cross-section balancing. *Journal of Structural Geology* **12,** 403–417.

Ramsay, J. G., Casey, M. and Kligfield, R. (1983) Role of shear in development of the Helvetic fold-thrust belt of Switzerland. *Geology* **11,** 439–442.

Royse, F. Jr., Warner, M. A. and Reese, D. L. (1975) *Thrust belt structural geometry and related stratigraphic problems Wyoming–Idaho–northern Utah.* Rocky Mountain Association. Geological. Symposium, Denver, pp. 41–54.

Sanderson, D. J. (1982) Models of strain variation in nappes and thrust sheets: a review. *Tectonophysics* **88,** 201–233.

Schwans, P. (1988) Depositional response of Pigeon Creek Formation, Utah, to initial fold-thrust belt deformation in a differentially subsiding foreland basin. In *Interaction of the Rocky Mountain Foreland and Cordilleran Thrust Belt*, ed. C. J. Schmidt and W. J. Perry, pp. 489–514. Geological Society of America Memoir, **171**.

Smith, R. B. and Bruhn, R. L. (1984) Intraplate extensional tectonics of the eastern Basin-Range: inferences on structural style from seismic reflection data, regional tectonics, and thermal–mechanical models of brittle–ductile deformation. *Journal of Geophysical Research* **89,** 5733–5762.

Stringham, B. F. (1942) Mineralization in the West Tintic mining district, Utah. *Geological Society of America Bulletin* **53,** 267–290.

Tooker, E. W. (1983) Variations in structural style and correlation of thrust plates in Sevier foreland thrust belt, Great Salt Lake area, Utah. In *Tectonic and Stratigraphic studies in the Eastern Great Basin*, ed. D. M. Miller, V. R. Todd and K. A. Howard, pp. 61–74. Geological Society of America Memoir, **157**.

Wojtal, S. (1986) Deformation within foreland thrust sheets by population of minor faults. *Journal of Structural Geology* **8,** 341–360.

Woodward, N. B., (1985) ed., Valley and Ridge thrust belt: Balanced structural sections, Pennsylvania to Alabama, University of Tennessee, Department of Geological Science, *Studies in Geology*, **12**, 64 pp.

Woodward, N. B., Boyer, S. E. and Suppe, J. (1989) Balanced Geological Cross Sections: An essential technique in geological research and exploration. *28th International Geological Congress, Short Course in Geology*. American Geophysical Union.

Yonkee, W. A. (1992) Basement-cover relations, Sevier orogenic belt, northern Utah. *Geological Society of America Bulletin* **104,** 280–322.

Yonkee, W. A. and Mitra, G. (1993) Comparison of basement styles in the Rocky Mountain Foreland and Sevier Orogenic Belt. In *Basement behavior in Rocky Mountain foreland structure*, ed. C. Schmidt, R. Chase and E. Erslev, pp. 197–228. Geological Society of America Special Paper, **280**.

APPENDIX A

Strain Data From The Hanging Wall Of The Sheeprock Thrust North Of Indian Springs Fault. See Fig. 13 for locations

Location no.	Orientation of *X*-Axis	Orientation of *Y*-Axis	Orientation of *Z*-Axis	*RXY*	*RYZ*	*RXZ*
1	11.88, 150.00	59.19, 260.66	27.97, 053.59	1.15	1.08	1.25
2	10.87, 108.01	61.48, 218.69	26.02, 012.63	1.11	1.07	1.18
3	53.86, 357.25	04.14, 092.94	35.82, 185.93	1.12	1.18	1.33
4	38.34, 359.80	32.62, 120.21	34.73, 236.56	1.11	1.17	1.30
5	03.42, 216.73	03.14, 233.46	85.36, 004.64	1.09	1.13	1.23
6	18.20, 108.08	27.55, 217.95	56.08, 358.82	1.15	1.15	1.32
7	06.72, 084.30	64.26,188.45	24.72, 351.19	1.19	1.10	1.30
8	05.89, 302.66	64.96, 044.60	24.24, 210.00	1.15	1.17	1.34
9	46.99, 167.31	04.85, 262.53	42.60, 357.00	1.21	1.14	1.38
10	23.91, 216.60	66.01, 041.35	01.76, 307.39	1.14	1.08	1.23
11	08.58, 138.38	52.73, 036.95	35.94, 234.66	1.06	1.15	1.22
12	11.56, 225.86	32.79, 128.28	54.72, 332.67	1.05	1.11	1.16
13	01.37, 265.66	04.56, 175.55	85.24, 012.30	1.19	1.10	1.31
14	68.87, 025.30	06.44, 278.35	20.04, 185.96	1.1	1.17	1.29
15	05.76, 161.80	26.39, 068.93	62.89, 263.15	1.07	1.05	1.13
16	43.34, 269.54	46.47, 082.98	03.28, 176.44	1.13	1.17	1.32
17	19.60, 207.10	02.97, 116.04	70.16, 017.78	1.18	1.04	1.22
18	05.44, 205.03	79.53, 326.04	08.92, 114.18	1.07	1.19	1.28
19	03.57, 097.20	59.23, 001.18	30.52, 189.31	1.11	1.14	1.26
20	21.06, 133.77	43.18, 244.95	39.38, 025.34	1.13	1.08	1.23
21	10.00, 041.39	27.10, 306.22	60.82, 149.80	1.13	1.19	1.35
22	13.67, 212.94	40.21, 111.07	46.56, 317.82	1.04	1.08	1.13
23	08.09, 028.28	41.56, 125.52	47.30, 289.42	1.17	1.05	1.23
24	03.81, 046.93	39.36, 313.80	50.38, 141.55	1.17	1.09	1.27
25	37.74, 104.94	24.90, 216.00	42.02, 330.72	1.21	1.16	1.40
26	78.60, 241.98	10.26, 088.98	04.91, 357.20	1.29	1.02	1.32
27	09.21, 276.11	74.21, 151.14	12.72, 008.20	1.15	1.09	1.25
28	24.11, 249.08	24.27, 147.44	54.59, 019.08	1.1	1.09	1.20
29	56.84, 252.55	06.06, 351.90	32.45, 085.78	1.19	1.14	1.36

Continued overleaf

Location no.	Orientation of *X*-Axis	Orientation of *Y*-Axis	Orientation of *Z*-Axis	*RXY*	*RYZ*	*RXZ*
30	11.44, 178.03	48.02, 075.04	39.70, 277.70	1.09	1.14	1.24
31	22.80, 351.40	38.91, 241.57	42.44, 104.00	1.08	1.06	1.15
32	48.21, 255.96	18.31, 007.69	35.99, 111.59	1.18	1.1	1.3
33	15.32, 073.97	08.35, 166.27	72.45, 283.93	1.1	1.11	1.22
34	41.83, 130.49	32.84, 005.20	30.74, 252.64	1.06	1.08	1.14
35	17.13, 297.10	41.86, 191.07	43.16, 043.90	1.12	1.24	1.38
36	60.94, 109.45	28.08, 305.63	06.86, 211.95	1.18	1.1	1.3
37	78.25, 194.36	04.67, 307.49	10.76, 038.38	1.14	1.19	1.36
38	14.16, 031.01	13.96, 124.61	69.90, 257.41	1.1	1.05	1.16
39	02.66, 326.79	74.59, 066.48	15.16, 236.07	1.24	1.05	1.31
40	32.77, 131.63	49.82, 351.97	20.56, 235.60	1.09	1.18	1.28
41	17.94, 295.88	37.73, 040.38	46.76, 185.76	1.15	1.19	1.37
42	56.56, 019.87	22.81, 149.42	23.06, 249.73	1.34	1.11	1.48
43	74.04, 318.04	09.35, 192.92	12.82, 100.77	1.18	1.08	1.27
44	08.05, 250.09	79.16, 112.47	07.21, 341.12	1.2	1.09	1.31
45	25.36, 018.18	05.95, 111.02	63.85, 213.28	1.04	1.3	1.35
46	23.76, 268.59	44.43, 024.16	36.13, 159.85	1.04	1.16	1.21
47	06.16, 212.26	28.51, 118.90	60.71, 313.36	1.1	1.18	1.3
48	43.43, 261.37	06.73, 164.95	45.78, 067.99	1.08	1.2	1.3
49	23.58, 125.75	43.36, 240.09	37.38, 016.27	1.14	1.16	1.32
50	54.12, 088.48	00.53, 179.21	35.88, 269.59	1.14	1.16	1.32
51	23.41, 160.38	49.62, 039.78	30.78, 265.33	1.09	1.18	1.28
52	28.96, 132.55	32.84, 243.47	43.37, 011.04	1.22	1.04	1.27
53	24.22, 108.98	40.92, 221.93	39.39, 357.31	1.25	1.07	1.34
54	50.93, 192.69	34.49, 044.88	16.07, 303.47	1.17	1.37	1.6
55	53.43, 046.97	06.76, 146.16	35.74, 241.06	1.21	1.27	1.53
56	15.22, 308.47	63.64, 071.76	20.99, 212.48	1.18	1.07	1.27

Strain Data From The Hanging Wall Of The Sheeprock Thrust South Of Indian Springs Fault

Location no.	Orientation of *X*-Axis	Orientation of *Y*-Axis	Orientation of *Z*-Axis	*RXY*	*RYZ*	*RXZ*
1	29.03, 163.29	02.65, 071.82	60.83, 337.07	1.13	1.08	1.22
2	28.03, 140.57	47.92, 266.70	28.54, 033.74	1.15	1.35	1.56
3	35.58, 284.26	53.88, 117.58	06.36, 018.80	1.23	1.18	1.45
4	61.46, 058.17	28.39, 244.62	02.70, 153.15	1.11	1.09	1.22
5	56.44, 106.48	22.85, 235.91	23.17, 336.30	1.21	1.15	1.38
6	05.78, 278.30	56.17, 179.62	33.20, 012.10	1.12	1.22	1.37
7	44.86, 051.97	03.98, 145.94	44.86, 239.91	1.17	1.06	1.24
8	00.78, 248.51	81.00, 153.61	08.96, 338.64	1.17	1.22	1.43
9	17.17, 316.06	21.88, 053.18	61.62, 191.18	1.06	1.19	1.25
10	14.16, 159.39	40.53, 261.85	46.02, 054.22	1.04	1.08	1.12
11	19.08, 019.97	22.84, 281.59	59.50, 145.92	1.07	1.05	1.12
12	02.30, 207.22	05.85, 297.45	83.71, 095.81	1.19	1.32	1.56
13	25.09, 317.48	52.18, 190.39	26.30, 060.86	1.09	1.07	1.17
14	46.51, 344.88	09.97, 085.56	41.76, 184.60	1.16	1.14	1.32
15	51.21, 075.37	04.70, 171.24	38.39, 264.97	1.62	1.2	1.94
16	00.30, 176.52	39.13, 086.27	50.87, 266.88	1.23	1.19	1.46
17	06.68, 176.56	48.27, 079.02	40.95, 272.39	1.24	1.35	1.67
18	28.67, 012.30	19.16, 271.34	54.46, 152.24	1.2	1.26	1.52
19	66.85, 253.95	06.18, 358.63	22.21, 091.16	1.49	1.23	1.84
20	05.11, 219.9	39.91, 125.61	49.63, 315.94	1.25	1.46	1.81
21	00.03, 123.49	54.77, 033.45	35.23, 213.51	1.13	1.36	1.53
22	17.16, 329.59	57.41, 210.71	26.79, 068.56	1.07	1.63	1.75
23	65.86, 060.47	18.48, 282.24	14.98, 187.11	1.26	1.58	2
24	04.25, 021.61	19.18, 290.13	70.32, 123.60	1.47	1.37	2
25	13.84, 070.62	16.79, 336.36	67.97, 198.13	1.09	1.07	1.17
26	06.84, 221.52	75.48, 103.92	12.75, 313.07	1.27	1.05	1.33
27	35.17, 306.18	00.68, 36.66	54.83, 127.63	1.42	1.54	2.19
28	04.01, 173.98	05.72, 83.57	83.01, 298.86	1.15	1.36	1.57

Strain Data From The Footwall Of The Sheeprock Thrust North Of Indian Springs Fault

Location no.	Orientation of *X*-Axis	Orientation of *Y*-Axis	Orientation of *Z*-Axis	*RXY*	*RYZ*	*RXZ*
1	10.67, 016.62	19.63, 110.47	67.45, 259.65	1.15	1.37	1.58
2	30.92, 095.19	08.98, 359.75	57.52, 255.38	1.12	1.23	1.38
3	36.06, 068.10	16.41, 170.49	49.24, 280.46	1.05	1.37	1.44
4	31.10, 115.13	06.57, 209.12	58.06, 309.76	1.13	1.26	1.42
5	21.40, 045.42	08.90, 138.94	66.65, 250.21	1.1	1.34	1.46
6	22.61, 287.63	13.55, 191.87	63.24, 073.31	1.15	1.26	1.45

Location no.	Orientation of *X*-Axis	Orientation of *Y*-Axis	Orientation of *Z*-Axis	*RXY*	*RYZ*	*RXZ*
7	03.68, 098.68	61.08, 195.35	28.64, 006.67	1.17	1.12	1.3
8	36.05, 048.54	38.95, 282.51	30.57, 163.99	1.08	1.58	1.71
9	34.09, 115.15	27.17, 135.47	43.70, 254.84	1.18	1.32	1.56
10	06.74, 010.25	11.71, 101.66	76.44, 250.90	1.12	1.27	1.42
11	20.20, 196.64	03.18, 287.81	69.53, 026.38	1.18	1.55	1.83
12	13.79, 212.78	15.78, 306.76	68.81, 083.53	1.31	1.37	1.79
13	34.22, 065.83	07.91, 330.41	54.62, 229.13	1.38	1.14	1.57
14	12.43, 005.36	13.86, 098.48	71.21, 234.96	1.16	1.38	1.6
15	09.76, 330.79	35.55, 067.85	52.73, 227.73	1.32	1.22	1.62
16	29.99, 088.22	59.63, 278.29	04.39, 180.76	1.04	1.35	1.4
17	16.37, 045.65	01.33, 315.26	73.58, 220.75	1.18	1.52	1.79
18	13.88, 224.52	62.78, 105.81	22.92, 320.52	1.1	1.43	1.57
19	17.31, 177.50	07.20, 085.25	71.16, 333.51	1.21	1.21	1.47
20	44.36, 124.92	40.34, 271.07	17.67, 016.77	1.04	1.18	1.22
21	06.36, 022.38	00.22, 292.36	83.63, 200.37	1.16	1.4	1.63
22	18.60, 205.89	30.37, 104.51	53.29, 322.71	1.13	1.4	1.58
23	07.46, 184.22	27.59, 278.15	61.25, 080.41	1.21	1.24	1.5
24	00.50, 268.47	01.62, 358.48	88.30, 161.28	1.09	1.14	1.24
25	31.58, 135.86	04.31, 043.21	58.05, 306.26	1.16	1.43	1.67
26	58.51, 171.63	12.41, 060.59	28.44, 323.75	1.08	1.11	1.2
27	20.36, 190.57	03.80, 099.16	69.26, 359.07	1.18	1.22	1.44
28	06.56, 314.48	36.22, 219.65	53.00, 053.26	1.06	1.18	1.25
29	14.34, 120.10	11.70, 213.13	71.33, 340.93	1.3	1.14	1.49
30	06.13, 165.98	03.28, 256.33	83.04, 014.34	1.27	1.05	1.34
31	35.36, 221.73	50.12, 009.87	16.02, 119.97	1.53	1.24	1.88
32	29.30, 000.20	25.20, 254.88	49.56, 131.37	1.24	1.24	1.54
33	08.03, 067.12	03.40, 336.64	81.27, 223.90	1.22	1.39	1.69
34	34.80, 191.07	07.81, 095.60	54.08, 354.69	1.11	1.45	1.6
35	00.99, 068.25	13.11, 158.48	76.85, 334.01	1.08	1.23	1.33
36	44.21, 272.78	14.06, 168.68	42.40, 065.45	1.09	1.09	1.2
37	22.14, 292.10	07.74, 025.27	66.41, 133.39	1.13	1.28	1.44
38	32.59, 196.21	00.21, 106.07	57.41, 015.74	1.13	1.43	1.62
39	30.07, 169.57	09.69, 073.89	58.09, 327.98	1.05	1.52	1.6
40	24.72, 029.46	31.88, 136.09	47.66, 269.12	1.28	1.11	1.42
41	33.76, 014.04	37.08, 253.69	34.92, 131.85	1.25	1.17	1.46
42	02.23, 227.74	81.59, 122.47	08.10, 311.94	1.09	1.05	1.15
43	28.65, 070.96	55.27, 288.96	17.93, 171.14	1.11	1.24	1.37

APPENDIX B

Strain Data (Modified) From The Hanging Wall Of Sheeprock Thrust North Of Indian Springs Fault

Location no.	Orientation of *X*-Axis	Orientation of *Y*-Axis	Orientation of *Z*-Axis	*RXY*	*RYZ*	*RXZ*
1	59.19, 260.66	11.88, 150.00	27.97, 053.59	0.87	1.25	1.08
2	61.48, 218.69	10.87, 108.01	26.02, 012.63	0.9	1.18	1.07
3	04.14, 092.94	53.86, 357.25	35.82, 185.93	0.89	1.33	1.18
4	32.62, 120.21	38.34, 359.80	34.73, 236.56	0.9	1.30	1.17
5	03.14, 233.46	03.42, 216.73	85.36, 004.64	0.92	1.23	1.13
6	27.55, 217.95	18.20, 108.08	56.08, 358.82	0.87	1.32	1.15
7	06.72, 084.30	64.26,188.45	24.72, 351.19	1.19	1.10	1.30
8	64.96, 044.60	05.89, 302.66	24.24, 210.00	0.87	1.34	1.17
9	04.85, 262.53	46.99, 167.31	42.60, 357.00	0.83	1.38	1.14
10	66.01, 041.35	23.91, 216.60	01.76, 307.39	0.88	1.23	1.08
11	52.73, 036.95	08.58, 138.38	35.94, 234.66	0.94	1.22	1.15
12	32.79, 128.28	11.56, 225.86	54.72, 332.67	0.95	1.16	1.11
13	01.37, 265.66	04.56, 175.55	85.24, 012.30	1.19	1.10	1.31
14	06.44, 278.35	68.87, 025.30	20.04, 185.96	0.91	1.29	1.17
15	26.39, 068.93	05.76, 161.80	62.89, 263.15	0.93	1.13	1.05
16	43.34, 269.54	46.47, 082.98	03.28, 176.44	1.13	1.17	1.32
17	02.97, 116.04	19.60, 207.10	70.16, 017.78	0.85	1.22	1.04
18	79.53, 326.04	05.44, 205.03	08.92, 114.18	0.93	1.28	1.19
19	03.57, 097.20	59.23, 001.18	30.52, 189.31	1.11	1.14	1.26
20	43.18, 244.95	21.06, 133.77	39.38, 025.34	0.88	1.23	1.08
21	27.10, 306.22	10.00, 041.39	60.82, 149.80	0.88	1.35	1.19
22	40.21, 111.07	13.67, 212.94	46.56, 317.82	0.96	1.13	1.08
23	41.56, 125.52	08.09, 028.28	47.30, 289.42	0.85	1.23	1.05
24	03.81, 046.93	39.36, 313.80	50.38, 141.55	1.17	1.09	1.27
25	24.90, 216.00	37.74, 104.94	42.02, 330.72	0.83	1.40	1.16
26	78.60, 241.98	10.26, 088.98	04.91, 357.20	1.29	1.02	1.32
27	09.21, 276.11	74.21, 151.14	12.72, 008.20	1.15	1.09	1.25
28	24.11, 249.08	24.27, 147.44	54.59, 018.08	1.1	1.09	1.20

Continued overleaf

Location no.	Orientation of *X*-Axis	Orientation of *Y*-Axis	Orientation of *Z*-Axis	*RXY*	*RYZ*	*RXZ*
29	56.84, 252.55	06.06, 351.90	32.45, 085.78	1.19	1.14	1.36
30	48.02, 075.04	11.44, 178.03	39.70, 277.70	0.92	1.24	1.14
31	38.91, 241.57	22.80, 351.40	42.44, 104.00	0.93	1.15	1.06
32	48.21, 255.96	18.31, 007.69	35.99, 111.59	1.18	1.1	1.3
33	15.32, 073.97	08.35, 166.27	72.45, 283.93	1.1	1.11	1.22
34	32.84, 005.20	41.83, 130.49	30.74, 252.64	0.94	1.14	1.08
35	41.86, 191.07	17.13, 297.10	43.16, 043.90	0.89	1.38	1.24
36	28.08, 305.63	60.94, 109.45	06.86, 211.95	0.85	1.3	1.1
37	04.67, 307.49	78.25, 194.36	10.76, 038.38	0.88	1.36	1.19
38	13.96, 124.61	14.16, 031.01	69.90, 257.41	0.91	1.16	1.05
39	74.59, 066.48	02.66, 326.79	15.16, 236.07	0.81	1.31	1.05
40	49.82, 351.97	32.77, 131.63	20.56, 235.60	0.92	1.28	1.18
41	17.94, 295.88	37.73, 040.38	46.76, 185.76	1.15	1.19	1.37
42	22.81, 149.42	56.56, 019.87	23.06, 249.73	0.75	1.48	1.11
43	09.35, 192.92	74.04, 318.04	12.82, 100.77	0.85	1.27	1.08
44	08.05, 250.09	79.16, 112.47	07.21, 341.12	1.2	1.09	1.31
45	05.95, 111.02	25.36, 018.18	63.85, 213.28	0.96	1.35	1.3
46	23.76, 268.59	44.43, 024.16	36.13, 159.85	1.04	1.16	1.21
47	28.51, 118.90	06.16, 212.26	60.71, 313.36	0.91	1.3	1.18
48	43.43, 261.37	06.73, 164.95	45.78, 067.99	1.08	1.2	1.3
49	43.36, 240.09	23.58, 125.75	37.38, 016.27	0.88	1.32	1.16
50	54.12, 088.48	00.53, 179.21	35.88, 269.59	1.14	1.16	1.32
51	49.62, 039.78	23.41, 160.38	30.78, 265.33	0.92	1.28	1.18
52	32.84, 243.47	28.96, 132.55	43.37, 011.04	0.82	1.27	1.04
53	40.92, 221.93	24.22, 108.98	39.39, 357.31	0.8	1.34	1.07
54	34.49, 044.88	50.93, 192.69	16.07, 303.47	0.86	1.6	1.37
55	53.43, 046.97	06.76, 146.16	35.74, 241.06	1.21	1.27	1.53
56	63.64, 071.76	15.22, 308.47	20.99, 212.48	0.85	1.27	1.07

Strain Data (Modified) From The Hanging Wall Of Sheeprock Thrust South Of Indian Springs Fault

Location no.	Orientation of *X*-Axis	Orientation of *Y*-Axis	Orientation of *Z*-Axis	*RXY*	*RYZ*	*RXZ*
1	02.65, 071.82	29.03, 163.29	60.83, 337.07	0.89	1.22	1.08
2	47.92, 266.70	28.03, 140.57	28.54, 033.74	0.87	1.56	1.35
3	53.88, 117.58	35.58, 284.26	06.36, 018.80	0.81	1.45	1.18
4	61.46, 058.17	28.39, 244.62	02.70, 153.15	1.11	1.09	1.22
5	22.85, 235.91	56.44, 106.48	23.17, 336.30	0.83	1.38	1.15
6	56.17, 179.62	05.78, 278.30	33.20, 012.10	0.89	1.37	1.22
7	44.86, 051.97	03.98, 145.94	44.86, 239.91	1.17	1.06	1.24
8	00.78, 248.51	81.00, 143.61	08.96, 338.64	1.17	1.22	1.43
9	21.88, 053.18	17.17, 316.06	61.62, 191.18	0.94	1.25	1.19
10	40.53, 261.85	14.16, 159.39	46.02, 054.22	0.96	1.12	1.08
11	22.84, 281.59	19.08, 019.97	59.50, 145.92	0.93	1.12	1.05
12	05.85, 297.45	02.30, 207.22	83.71, 095.81	0.84	1.56	1.32
13	52.18, 190.39	25.09, 317.48	26.30, 060.86	0.92	1.17	1.07
14	09.97, 085.56	46.51, 344.88	41.76, 184.60	0.86	1.32	1.14
15	51.21, 075.37	04.70, 171.24	38.39, 264.97	1.62	1.2	1.94
16	39.13, 086.27	00.30, 176.52	50.87, 266.88	0.81	1.46	1.19
17	48.27, 079.02	06.68, 176.56	40.95, 272.39	0.81	1.67	1.35
18	19.16, 271.34	28.67, 012.30	54.46, 152.24	0.83	1.52	1.26
19	66.85, 253.95	06.18, 358.63	22.21, 091.16	1.49	1.23	1.84
20	05.11, 219.9	39.91, 125.61	49.63, 315.94	1.25	1.46	1.81
21	54.77, 033.45	00.03, 123.49	35.23, 213.51	0.89	1.53	1.36
22	57.41, 210.71	17.16, 329.59	26.79, 068.56	0.93	1.75	1.63
23	65.86, 060.47	18.48, 282.24	14.98, 187.11	1.26	1.58	2
24	19.18, 290.13	04.25, 021.61	70.32, 123.60	0.68	2	1.37
25	13.84, 070.62	16.79, 336.36	67.97, 198.13	1.09	1.07	1.17
26	75.48, 103.92	06.84, 221.52	12.75, 313.07	0.79	1.33	1.05
27	00.68, 36.66	35.17, 306.18	54.83, 127.63	0.7	2.19	1.54
28	05.72, 83.57	04.01, 173.98	83.01, 298.86	0.87	1.57	1.36

Strain Data (Modified) From The Footwall Of Sheeprock Thrust North Of Indian Springs Fault

Location no.	Orientation of *X*-Axis	Orientation of *Y*-Axis	Orientation of *Z*-Axis	*RXY*	*RYZ*	*RXZ*
1	19.63, 110.47	10.67, 016.62	67.45, 259.65	0.89	1.58	1.37
2	08.98, 359.75	30.92, 095.19	57.52, 255.38	0.89	1.38	1.23
3	36.06, 068.10	16.41, 170.49	49.24, 280.46	1.05	1.37	1.44
4	06.57, 209.12	31.10, 115.13	58.06, 309.76	0.88	1.42	1.26
5	21.40, 045.42	08.90, 138.94	66.65, 250.21	1.1	1.34	1.46
6	13.55, 191.87	22.61, 287.63	63.24, 073.31	0.89	1.45	1.26

Location no.	Orientation of *X*-Axis	Orientation of *Y*-Axis	Orientation of *Z*-Axis	*RXY*	*RYZ*	*RXZ*
7	61.08, 195.35	03.68, 098.68	28.64, 006.67	0.86	1.3	1.12
8	36.05, 048.54	38.95, 282.51	30.57, 163.99	1.08	1.58	1.71
9	27.17, 135.47	34.09, 115.15	43.70, 254.84	0.85	1.56	1.32
10	11.71, 101.66	06.74, 010.25	76.44, 250.90	0.89	1.42	1.27
11	03.18, 287.81	20.20, 196.64	69.53, 026.38	0.85	1.83	1.55
12	15.78, 306.76	13.79, 212.78	68.81, 083.53	0.76	1.79	1.37
13	34.22, 065.83	07.91, 330.41	54.62, 229.13	1.38	1.14	1.57
14	13.86, 098.48	12.43, 005.36	71.21, 234.96	0.86	1.6	1.38
15	35.55, 067.85	09.76, 330.79	52.73, 227.73	0.76	1.62	1.22
16	29.99, 088.22	59.63, 278.29	04.39, 180.76	1.04	1.35	1.4
17	16.37, 045.65	01.33, 315.26	73.58, 220.75	1.18	1.52	1.79
18	13.88, 224.52	62.78, 105.81	22.92, 320.52	1.1	1.43	1.57
19	07.20, 085.25	17.31, 177.50	71.16, 333.51	0.83	1.47	1.21
20	40.34, 271.07	44.36, 124. 92	17.67, 016.77	0.96	1.22	1.18
21	00.22, 292.36	06.36, 022.38	83.63, 200.37	0.86	1.63	1.4
22	30.37, 104.51	18.60, 205.89	53.29, 322.71	0.88	1.58	1.4
23	27.59, 278.15	07.46, 184.22	61.25, 080.41	0.83	1.5	1.24
24	00.50, 268.47	01.62, 358.48	88.30, 161.28	1.09	1.14	1.24
25	04.31, 043.21	31.58, 135.86	58.05, 306.26	0.86	1.67	1.43
26	12.41, 060.59	58.51, 171.63	28.44, 323.75	0.93	1.2	1.11
27	03.80, 099.16	20.36, 190.57	69.26, 359.07	0.85	1.44	1.22
28	36.22, 219.65	06.56, 314.48	53.00, 053.26	0.94	1.25	1.18
29	11.70, 213.13	14.34, 120.10	71.33, 340.93	0.77	1.49	1.14
30	03.28, 256.33	06.13, 165.98	83.04, 014.34	0.79	1.34	1.05
31	50.12, 009.87	35.36, 221.73	16.02, 119.97	0.65	1.88	1.24
32	25.20, 254.88	29.30, 000.20	49.56, 131.37	0.81	1.54	1.24
33	03.40, 336.64	08.03, 067.12	81.27, 223.90	0.82	1.69	1.39
34	07.81, 095.60	34.80, 191.07	54.08, 354.69	0.9	1.6	1.45
35	00.99, 068.25	13.11, 158.48	76.85, 334.01	1.08	1.33	1.23
36	44.21, 272.78	14.06, 168.68	42.40, 065.45	1.09	1.09	1.2
37	07.74, 025.27	22.14, 292.10	66.41, 133.39	0.89	1.28	1.44
38	00.21, 106.07	32.59, 196.21	57.41, 015.74	0.89	1.62	1.43
39	09.69, 073.89	30.07, 169.57	58.09, 327.98	0.95	1.6	1.52
40	31.88, 136.09	24.72, 029.46	47.66, 269.12	0.78	1.42	1.11
41	37.08, 253.69	33.76, 014.04	34.92, 131.85	0.8	1.46	1.17
42	81.59, 122.47	02.23, 227.74	08.10, 311.94	0.92	1.15	1.05
43	55.27, 288.96	28.65, 070.96	17.93, 171.14	0.9	1.37	1.24